J. Fluid Mech. (1995) *vol.* 288, *pp.* 1–35

Experimental observations of edge waves

By S. J. BUCHAN[1] AND W. G. PRITCHARD[2]†

[1] Steedman Science & Engineering, 31 Bishop St., Jolimont, Western Australia, 6014

[2] Department of Mathematics, Penn State University, University Park, PA 16802, USA

(Received 18 November 1993 and in revised form 11 April 1994)

The main purpose of this paper is to provide some carefully documented experimental observations of the subharmonic generation of edge waves over a plane beach by waves normally incident on the beach from the distant ocean. In order to establish experimentally the details of the subharmonic instability mechanism, it is important first to determine the properties of the primary wave field whose stability is to be investigated. Thus, a detailed appraisal has been made of the wave field established in the tank and over the beach in the absence of edge waves. These data have been particularly useful in defining the amplitudes of the incident- and reflected-wave fields at the toe of the beach, the magnitudes of which are central to the triggering of the edge-wave instability. Details are presented of the edge-wave field over the beach, as well as marginal stability curves and initial growth rates of the instability, the latter two of which are compared with theoretical estimates obtained from extant theories of the instability mechanism. Some experiments are also described in which edge waves were established as modes forced by topographical imperfections at the beach.

1. Introduction

In 1952 Ursell demonstrated experimentally the possibility of edge-wave modes over a plane beach. Theoretically the amplitude of such a wave decays exponentially at large distances from the shoreline, precluding the possibility of generating it directly by forcing at large distances, and so Ursell generated the mode by forcing at the beach. However, it was shown experimentally by Galvin in the mid 1960s that edge waves could be generated through a nonlinear interaction mechanism by a wave train incident normally on the beach from large distances. The edge waves generated in this manner had half the frequency of the primary wave train, implying that the generation mechanism was surely a nonlinear process. This generation process was subsequently confirmed by several workers including Birchfield & Galvin (1975), Guza & Inman (1975), and Guza & Bowen (1976).

Theoretical explanations for the above generation mechanism for edge waves have been given, for example, by Guza & Davis (1974), Guza & Bowen (1976), Minzoni & Whitham (1977), Rockliff (1978) and Miles (1990*a*). In each of these studies the stability of a normally-incident-wave field to edge-wave perturbations was considered. Most of the studies assumed that the flows could be described by the irrotational motion of an inviscid fluid, with the incident wave field being, of necessity, a standing-wave field. The two exceptions are the papers of Guza & Bowen (1976) and Miles (1990*b*) in which allowance is made for imperfect reflection as a result of viscous effects in boundary layers on the sloping beach. The importance of viscous effects on the wave

† Dr Pritchard died while the paper was being printed.

motions over a beach has been highlighted by Mahony & Pritchard (1980) who showed that the primary wave field deduced on the basis of an inviscid model provides a very poor representation of wave fields observed in practical situations, even when there is no wave breaking over the beach. Even so, it would appear that a basic mechanism for the transfer of energy to the edge-wave field has been clearly established and the models do indeed capture several aspects of the experiments to be described. There are, however, some important features of the observed motions that are not well-predicted by the various models.

Following the original experimental demonstration of the possibility of edge waves by Ursell (1952) there have been several other experimental studies reported in the literature including works by Guza & Davis (1974), Birchfield & Galvin (1975), Guza & Inman (1975), Guza & Bowen (1976), Yeh (1986) and Lin (1988). Most of these have been concerned with the generation process by waves incident from the ocean, but in the study by Yeh the waves were generated directly at the beach, as had been done by Ursell. Yeh made careful measurements, in a relatively large-scale experiment, of a number of properties of the edge-wave field and found that several of his observations were in significant disagreement with the extant theoretical models. For example, the predicted magnitude of the set-down phenomenon of the mean water level was only half that observed experimentally, and the predicted offshore leakage rates of standing edge waves grossly underestimated the observed rates of decay of the waves. Thus the applicability of the theoretical models to the laboratory situation must be brought seriously into question.

The interpretation of laboratory experiments concerning the run-up of waves on plane beaches requires considerable care, as illustrated by the following simple experiment. A plane wave, propagating along a uniform channel approaches a plane beach at normal incidence. When such a wave impinges on an accurately plane beach, aligned to be laterally horizontal to a high degree of accuracy, the wave run-up is, as expected, nearly uniform across the beach, an example of which is shown in figure 1. Figure 1(*a*) shows the shoreline with the wave near its point of maximum wash excursion, and figure 1(*b*) shows the shoreline at a time when the wave was near its lowest point on the beach. In the latter photograph the instantaneous shoreline appears as the more pronounced horizontal line, and the fainter line indicates the line of maximum excursion of the wave marked by the edge of the residual film of water left by the wave when it receded. (Note that the faint horizontal line appearing near the bottom of the photographs is associated with the construction of the beach and is not relevant to the interpretation of the fluid motions.) The nature of the wave motion over the beach can be changed dramatically, as indicated in the photographs of figure 2, by the apparently minor perturbation of allowing a small amount of leakage past the edges of the beach. Thus, the only difference between the conditions for the photographs shown in figure 1 and those of figure 2 was that a small gap of about 1 mm between the edges of the beach and the sidewalls of the channel in which the waves were generated had been sealed with a caulking compound for figure 1 and this had been removed for the other experiment. The forcing period (0.8800 s) for these motions happened to be reasonably close to the edge-wave period of 0.8556 s associated with one wavelength across the channel. Thus, it would appear that the motions shown in figure 2 were those of an edge wave forced by effects at the sides of the beach. But it is evident that, without the sealed-beach experiments, these waves could easily have been construed as arising from a nonlinear interaction associated with the incident wave field. It is felt that topographical forcing of wave modes such as the one shown in figure 2 is likely to be very important in the oceanographic context and, in particular,

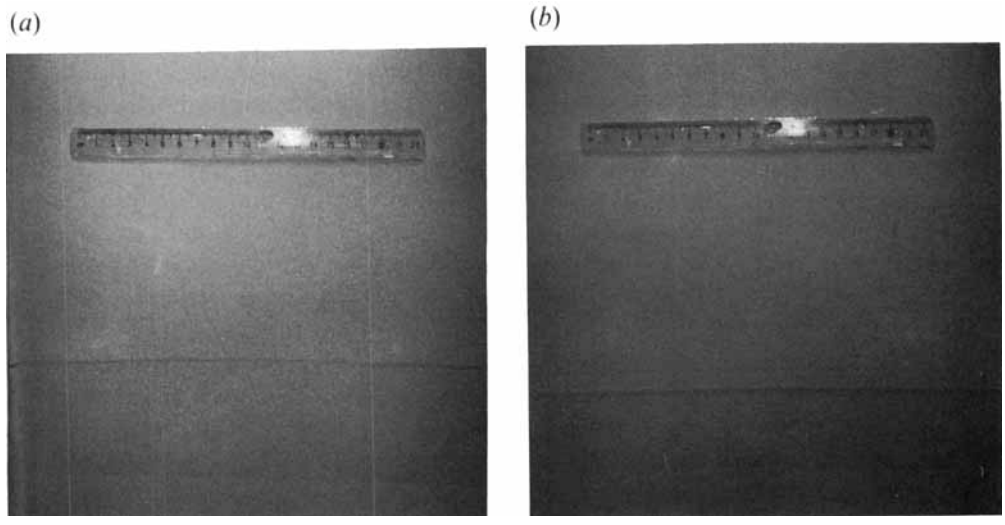

FIGURE 1. The shoreline of a plane wave normally incident on a plane beach of slope 15°. (*a*) The shoreline near the time of maximum wash excursion. (*b*) The shoreline near the time of minimum wash excursion. Also evident is the uppermost 'edge' of the residual film left from the run-up phase of the motion. The period of these motions was 0.8800 s and the water depth at the toe of the beach was 50 mm.

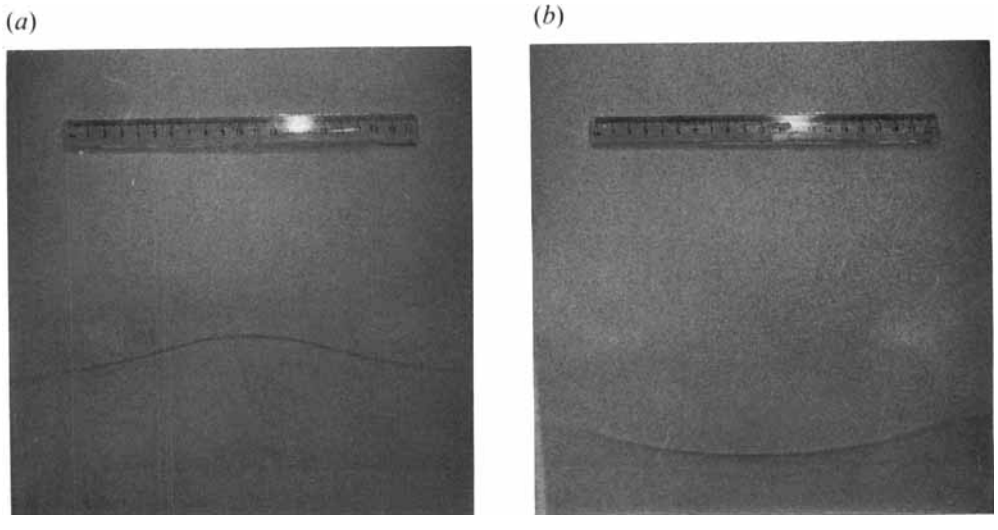

FIGURE 2. The shoreline of a plane wave normally incident on a plane beach of slope 15° for which there was a small gap between the edges of the beach and the walls of the tank in which the waves were generated. (*a*) The shoreline near the time of maximum wash excursion. (*b*) The shoreline near the time of minimum wash excursion. Also evident is the uppermost 'edge' of the residual film left from the run-up phase of the motion. The period of these motions was 0.8800 s and the water depth at the toe of the beach was 50 mm.

we shall demonstrate below how edge-wave modes can be excited easily through topographic forcing.

The main thrust of this work is the careful study of the establishment of edge waves over a sloping beach through the subharmonic resonant-interaction process referred to

above. To investigate the bifurcation process it is essential first to establish in some detail the properties of the primary wave field whose stability is to be investigated. Because of the scale on which these experiments were undertaken, the amplitude of the incident-wave train needed to excite the instability was quite large with the result that nonlinear effects played a not insignificant role in the evolution of these waves.

A complete interpretation of the experiments would be a somewhat daunting task and we have therefore decided simply to concentrate on outlining the main experimental findings. Thus, after providing some basic definitions, a careful description is given of the experimental apparatus and the procedures used to make the measurements. Then, in §4, we provide a summary of the primary wave fields in the uniform section of the channel and over the beach. In connection with these measurements, some numerical experiments are described (see the Appendix) which show the importance of dissipative effects in determining the structure of the observed longitudinal-wave fields and give a feel for their nonlinear properties. The measurements of the primary wave field will be used to prescribe an effective amplitude of the incident wave at the toe of the beach and an estimate of the relative magnitude of the reflected wave. While measurements of the basic wave field in the present situation might seem to be a somewhat routine exercise, the results were not without surprises. In particular, at $T \approx 0.43$ s, we observed a most unusual (and inexplicable to us) response for the longitudinal field. Details of edge-wave fields, generated through a parametrically forced (subharmonic) instability, are presented in §5. Here we give details of the edge-wave structure over the beach and of the effect of the edge wave on the longitudinal-wave field. Marginal stability curves, showing the critical incident-wave amplitude (as a function of wavemaker period) above which the instability grows, have been determined and are compared with theoretical estimates. The marginal stability curves reveal an unexpected lobe-like structure, which also is seen clearly in the measured growth rates of the instability. This unexpected structure appears to be associated with a secondary instability in which a longitudinal seiche of the entire tank is involved. Measurements of the equilibrium edge-wave amplitudes are also presented. In §6 some results are presented in which the edge waves were forced by a small transverse tilting of the beach, under which circumstances the parametric mechanism is not required and the waves arise through synchronous generation. In the concluding section we have tried to give a brief appraisal of what we feel are the most significant of our findings.

2. Basic definitions

The configuration with which we shall be concerned is depicted schematically in figure 3. Waves are generated by a plane wavemaker spanning a uniform channel of breadth b, filled with water to a depth H. The far end of the channel is terminated by a plane beach at an angle β to the horizontal. The experiments have been designed so that the waves generated in the uniform section of the channel have wavelength considerably larger than the water depth, and the main purpose of the study is to investigate the possible nonlinear generation of edge waves over the sloping beach.

We shall suppose that the wavemaker executes sinusoidal oscillations of period $T\,(=2\pi/\omega$, where ω is the frequency) and amplitude $\frac{1}{2}s$, and that it is located a distance L_0 from the toe of the beach, so that the distance L from the wavemaker to the shoreline is $L_0+H/\tan\beta$. The action of the wavemaker gives rise, basically, to a longitudinal-wave field of amplitude $\tilde{\zeta}_0(\tilde{x})\cos(\omega\tilde{t}+\theta_0(\tilde{x}))$, where $\tilde{x}$ denotes distance from the wavemaker, $\tilde{t}$ is time and θ_0 is a phase function. (We shall use the tilde to denote

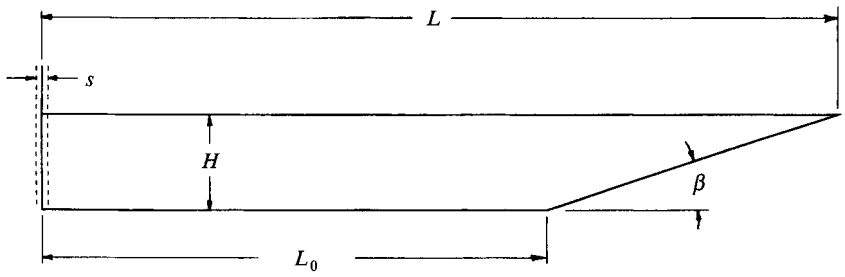

FIGURE 3. Schematic representation of the apparatus used in the experiments.

dimensional quantities: it will be convenient in describing the results to use different non-dimensionalizations for the motions in the uniform part of the channel and those over the beach, and these will be introduced at the appropriate time.) Also present in the tank will be a transverse wave motion of amplitude $\tilde{\zeta}_t(\tilde{x})\cos(\omega\tilde{t}+\theta_t(\tilde{x}))$, having a cross-channel wavenumber $l=\pi/b$. Typically the transverse wave field was small compared with the longitudinal field and forcing frequencies were such that other possible transverse modes were not observed. Let $\tilde{\xi}=L-\tilde{x}$ denote distance from the shoreline, let $\tilde{y}$ be the transverse coordinate, measured from the centreline of the channel, and let $\tilde{z}$ be the vertically upward coordinate, measured from the undisturbed free surface.

At special forcing frequencies, edge waves can arise over the sloping beach. We shall be concerned here only with the classic Stokes wave, whose edge-wave amplitude $\tilde{\eta}$ is given by

$$\tilde{\eta}(\tilde{\xi},\tilde{y},\tilde{t})=ag\,\mathrm{e}^{-k\tilde{\xi}\cos\beta}\cos(k\tilde{y}-\sigma\tilde{t}), \tag{1}$$

for which the dispersion relation relating the frequency σ to the wavenumber k is given by

$$\sigma^2=gk\sin\beta, \tag{2}$$

where g is the gravity constant and a represents the wave amplitude at the shoreline. (The Stokes wave is, of course, just one of a discrete set of possible modes, as shown by Ursell 1952.) It is seen from (1) that the wave amplitude decays exponentially with $\tilde{\xi}$ but, because of the finite extent of the beach in our experiments and also possibly as a consequence of nonlinear effects, the edge waves may extend into the uniform part of the channel. In keeping with the above notation we shall denote the amplitude of the edge-wave field by $\tilde{\eta}_0(\tilde{\xi})\cos(\sigma\tilde{t}+\theta_e(\tilde{\xi}))$. Let the dimensionless lengthscale ξ over the beach be given by $\xi=\tilde{\xi}\sigma^2/g\sin\beta$.

The edge wave may extend into the uniform part of the channel either as a decaying mode or as a radiating wave, effects which are described nicely by Mathew & Akylas (1990). It was shown by Guza & Bowen (1976) that a standing edge wave can leak energy to an outgoing progressive wave with zero cross-channel wavenumber and frequency 2σ (modulo a nonlinear detuning effect). In addition, transverse modes may radiate into the channel. Suppose that such a mode has wavenumber $\boldsymbol{k}=n\boldsymbol{l}+\boldsymbol{m}$, where $n=1,2,3,\ldots$ and $\boldsymbol{l}$ is directed across the channel and $\boldsymbol{m}$ is the longitudinal wavenumber. Then the dispersion relation in the uniform part of the channel demands that

$$\sigma^2=g|\boldsymbol{k}|\tanh(|\boldsymbol{k}|H). \tag{3}$$

For subharmonic generation of edge waves, $\sigma\approx\frac{1}{2}\omega$. It follows, for the Stokes wave, that $\boldsymbol{m}$ must be purely imaginary, so the mode is trapped close to the toe of the beach.

Indeed, it is only the higher harmonics ($n = 3$ or 4, depending on which member of the Ursell set of edge waves is considered) that can radiate as free waves.

3. Experimental apparatus and measuring techniques

3.1. *The wave tank*

The tank used for these experiments was a channel of length 6 m and of cross-section approximately 30 cm × 30 cm. The sidewalls and the bed of the tank consisted of sheets of plate glass supported on a timber base. The gaps between the sidewalls and the glass bottom were packed with a filling compound.

A levelling of the tank was carried out by measuring water depths with a finely pointed cone mounted on a micrometer screw, the micrometer being clamped to a small tripod. The micrometer was slowly screwed down until the tip of the cone just broke the water surface, providing a measurement of the 'local' water depth to within approximately ± 0.001 cm. After levelling, the maximum deviation of the bed of the tank from a mean horizontal plane was less than 0.03 cm, with the cross-channel deviation at any given location along the tank being less than 0.006 cm. The channel width was found to be 29.68 ± 0.08 cm, but an adhesive tape attached to the sidewalls reduced the effective width by approximately 0.1 cm. This tape was a finely woven cotton bandage with an adhesive backing. Because of the absorption of water by the cotton the effects of contact-line hysteresis were avoided, virtually eliminating the formation of capillary ripples by the wave action at the sidewalls of the tank.

The tank was filled to a depth of approximately 5 cm for most of the experiments described below, but a few measurements were made with a depth of 10 cm.

3.2. *The wavemaker*

The wavemaker consisted of a plane flap mounted on a horizontal shaft at a height 73.6 cm above the bed of the tank. A driving mechanism forced the flap to make sinusoidal oscillations of amplitude not exceeding about $\frac{1}{15}$ rad, the actual displacement of the flap being measured (to within $\pm 3\%$ at worst, and usually within $\pm 1\%$) by a dial gauge bearing directly on it. Care was taken to make the face of the paddle square across the channel and vertical at the mid-point of its oscillation. Because of the fairly small depths used in the experiments, the horizontal displacement of the paddle was only about 7% greater at the bed of the channel than at the water surface. Thus, for convenience, we shall refer to a mean horizontal displacement of the paddle, namely the displacement at mid-water depth, as the stroke s, with the amplitude of the oscillations being $\frac{1}{2}s$. The flap was specially stiffened against torsional flexure.

The face of the wavemaker was of acrylic sheet which had been lightly abraded with a fine emery paper to facilitate the retention of a film of water well above the nominal depth in the channel. As with the cotton bandage on the sidewalls of the tank, this film helped avoid the formation of capillary ripples. Strips of foam plastic were attached to the sides and bottom of the wavemaker to fill the gaps between the wavemaker and the tank, and to reduce the flow past the edges of the paddle. The wavemaker was located approximately 25 cm from the rear end of the channel.

The wavemaker was attached through a variable throw crank to the shaft of a (400 pole) stepping motor. The ratio of the length of the crank to its throw was over 300:1. The electrical pulses controlling the stepping motor were derived from a crystal oscillator with frequency stability better than 5 parts in 10^7. This provided such good frequency control for the driving mechanism that phase drifting of the wavemaker was of negligible importance.

3.3. *The beach*

Special care was taken with the construction of the beach to avoid, as much as possible, the formation of transverse waves by topographic irregularities at the beach. To ensure good wetting properties at the shoreline and to provide a planar surface, the upper part of the beach was made from a piece of 12 mm thick float glass. This glass plate rested on a brass carriage, part of which comprised the lower section of the beach, namely the initial 15 cm near the toe. At the toe, where the beach met the bed of the channel, the brass tapered to a thickness of 1.8 mm. The glass plate rested on four finely threaded screws which were such that the upper milled surface of the carriage and the upper surface of the glass lay in the same plane. When correctly adjusted the separation between the lower (brass) section of the beach and the glass was indiscernible to the touch. The carriage rested on the lower edge of the milled flat at the front of the brass section and on two threaded 'legs' which were used to set the slope of the beach. This adjustment, and the determination of the slope, were made on a precision surface table. The slope was measured to within 0.05° and the cross-channel slope was estimated to be less than 0.02°. When placed in the tank the beach was aligned so that the machined flat at the very toe of the brass carriage was perpendicular to the sidewalls of the tank. The experiments to be described were made with three different beach slopes, namely 5.71° (0.100 rad), 10.00° (0.175 rad), and 15.00° (0.262 rad).

Once the beach had been properly positioned in the tank, the 1–2 mm gaps between the beach and the sidewalls of the tank were sealed with an epoxy resin (containing a powdered-slate filler) which, when hardened, was abraded with emery paper to provide a smooth surface flush with the beach. The joint between the glass plate and the brass carriage was also sealed with this resin and it was used to 'extend' the plane of the beach down to the bed of the channel from the machined flat at the toe of the brass carriage. This construction gave a watertight seal between the beach and the channel. The intersection between the plane of the beach and the bed of the channel was located at a distance of 450.0 cm from the mean position of the front face of the wavemaker in all these experiments.

Prior to assembly, the upper surface of the glass plate had been roughened through abrasion with a fine carborundum paste so that a film of water could be retained by the beach well above the shoreline. The resin filler at the edges of the beach also had good wetting properties. In addition, the surface was rubbed lightly with a fine emery paper before each experiment to guarantee cleanliness and good wetting properties at the shoreline. Through the use of these precautions, the generation of capillary waves at the shoreline was not a problem.

3.4. *Wave measurements*

Measurements of the wave amplitudes were made using proximity transducers located just above the surface of the water. The principle on which the instrument is based is that of determining the capacitance of the air gap between the transducer (one capacitor plate) and the water surface (which effectively forms the second plate of the capacitor). The measured capacitance may be used to infer the distance of the water surface from the transducer. The electronics associated with the instrument (Wayne Kerr B731B proximity meter) provided an output voltage that varied linearly with the distance between the two electrodes, for separations up to about half the diameter of the transducer. The frequency response of the system extended from d.c. up to about 1 kHz.

The output voltage from the proximity meter was transferred to an ultraviolet chart

recorder, to provide a permanent record of the displacement of the water surface at the position of the transducer. Half the peak-to-peak amplitude of this waveform was used as a measure of the wave amplitude. The waves generated in the present study had amplitudes ranging between 0.005 cm and 0.5 cm. Two sizes of capacitance probes were used to measure them: one had a diameter of 1.1 cm and the other a diameter of 2.5 cm. When the waveforms were not sinusoidal in time, owing to nonlinear effects, it would have been better to make a Fourier decomposition of the record, but we judged that the motions did not differ enough from a sinusoid to warrant the additional effort, given the technological resources available to us, required for such a decomposition. Examples of the extent of the nonlinear structure of the motions are indicated in the Appendix.

Two such probes were mounted on a carriage, one over the centre of the channel and the other at a distance of 6.0 cm from the sidewall. The central probe was used to give an estimate of the longitudinal wave amplitude, and the difference in amplitudes recorded by the two probes was used to estimate the amplitudes of cross-channel waves. The differencing of the voltages from the two transducers was effected electronically, with the actual amplitudes reported herein being determined on the assumption that the cross-channel modes were half-cosine waveforms. For the differencing technique to be reliable, it is important that both transducers are located on the same phase lines of the longitudinal-wave field: we have tried to ensure this by registering the alignment of the carriage to the sidewalls of the channel, keeping the probes on a perpendicular to the walls irrespective of the position of the carriage along the channel.

The accuracy of the measurements of the longitudinal waves should have been better than 2%. It is difficult to make a reliable estimate for that of the cross-channel waves, since the accuracy is related to both the incident- and transverse-wave amplitudes. However, for the experiments in which cross-channel waves were of significance, we believe the wave amplitudes were determined to an accuracy of better than 10%.

3.5. *Procedure*

When the appropriate adjustments to the beach had been made, it was placed in the channel with the toe at a distance 450 cm from the wavemaker (cf. §3.3). The beach was then sealed in place and left until a new slope was needed. Immediately before each experiment the beach was given a light rub down with emery paper and surface films were skimmed off the water.

The depth of the water was then set to the desired value using the pointed micrometer gauge described in §3.1. This gauge was placed at a 'standard' location in the tank and water was gradually added or removed until the level was within 0.001 cm of the desired setting. Thus, although the channel bed was flat only to within 0.03 cm, the water level in the tank was set much more accurately, allowing good reproducibility of operating conditions.

Once the water level had been set, the wavemaker was turned on and the experiment begun. It was found that the experiment could be continued for about an hour without evaporation losses changing the depth by too much (i.e. by more than 0.001 cm) or without the accumulation of surface films having a significant influence on the wave motions.

4. Primary wave field

Here we describe some of the properties of the basic wave field in the channel and over the beach. The results are needed to indicate the nature of the primary motion whose stability is to be investigated.

4.1. *The wave field in the channel*

These motions can be viewed as being composed of the following waves. (i) A longitudinal-wave train, crested across the channel, which is generated at the wavemaker. This train propagates along the channel, being slowly dissipated in the process, and is partially absorbed on the beach at the far end of the channel. (ii) The train reflected from the beach, which travels back along the channel to be re-reflected at the wavemaker. (iii) A cross-channel motion generated partly at the wavemaker, partly by the reaction of the longitudinal motions to small geometric irregularities in the channel or possibly through forcing effects of surface tension at the walls of the channel arising from the passage of the longitudinal motions. We shall refer to this motion as the transverse component of the wave field. (iv) A non-propagating field, the so-called parasitic field, associated with the motion of the wavemaker, arising because the velocity structure imposed by the wavemaker is not the same as that in the freely propagating waves. This motion, which is localized near the wavemaker, would appear to have little impact on the present study. (v) A possible seiching motion associated with standing waves along the tank. (vi) A possible longitudinal or transverse wave motion resulting from radiation of the edge-wave field into the channel.

The steady wave field in the channel is established to accommodate a balance between the energy input at the wavemaker and the various losses from the wave motions. The energy input is related to the wave amplitude and the relative phase of the wavemaker and the motion of the water at the wavemaker. Since the phase and amplitude of the reflected-wave field depend crucially on the positioning of the beach and on the dissipative processes taking place over the beach, it is apparent that the action of the beach is important in determining the overall wave motion established in the tank.

4.1.1. *The wave field at a given location*

Measurements of these fields were of two kinds. One set of experiments concerned the development of the wave train as it propagated into still water, paying particular attention to the wave amplitudes well behind the leading crest, but prior to the return of the reflected wave field from the beach. The other set related to the steady amplitude field that was established in the channel. Examples of the results of such measurements are given in figure 4(*a–c*), where both the longitudinal-wave amplitude, $\zeta_0 := 2\tilde{\zeta}_0/s$, and the transverse-wave amplitudes, $\zeta_t := 2\tilde{\zeta}_t/s$, at $X\ (:= \tilde{x}/H) = 30.0$ (i.e. at a distance of 30 water depths from the wavemaker) are compared with the amplitudes of the longitudinal motions that would be expected on the basis of Havelock's linear wavemaker theory (e.g. see Wehausen & Laitone 1960 or Ursell, Dean & Yu 1960). Each of these figures corresponds to a different amplitude of forcing by the wavemaker. Marked on the figures are some of the periods relevant to the experiments: T_A, T_B, T_C correspond to forcing periods for the possible subharmonic generation of the (fundamental) Stokes edge wave over each of the three beaches used in the experiments, and the periods T_n, $n = \frac{1}{2}, 1, \frac{3}{2}, 2$, correspond to natural periods of oscillation for modes with n wavelengths across the channel. In these figures the solid black symbols denote the amplitudes of the longitudinal motions and the open symbols give the transverse-

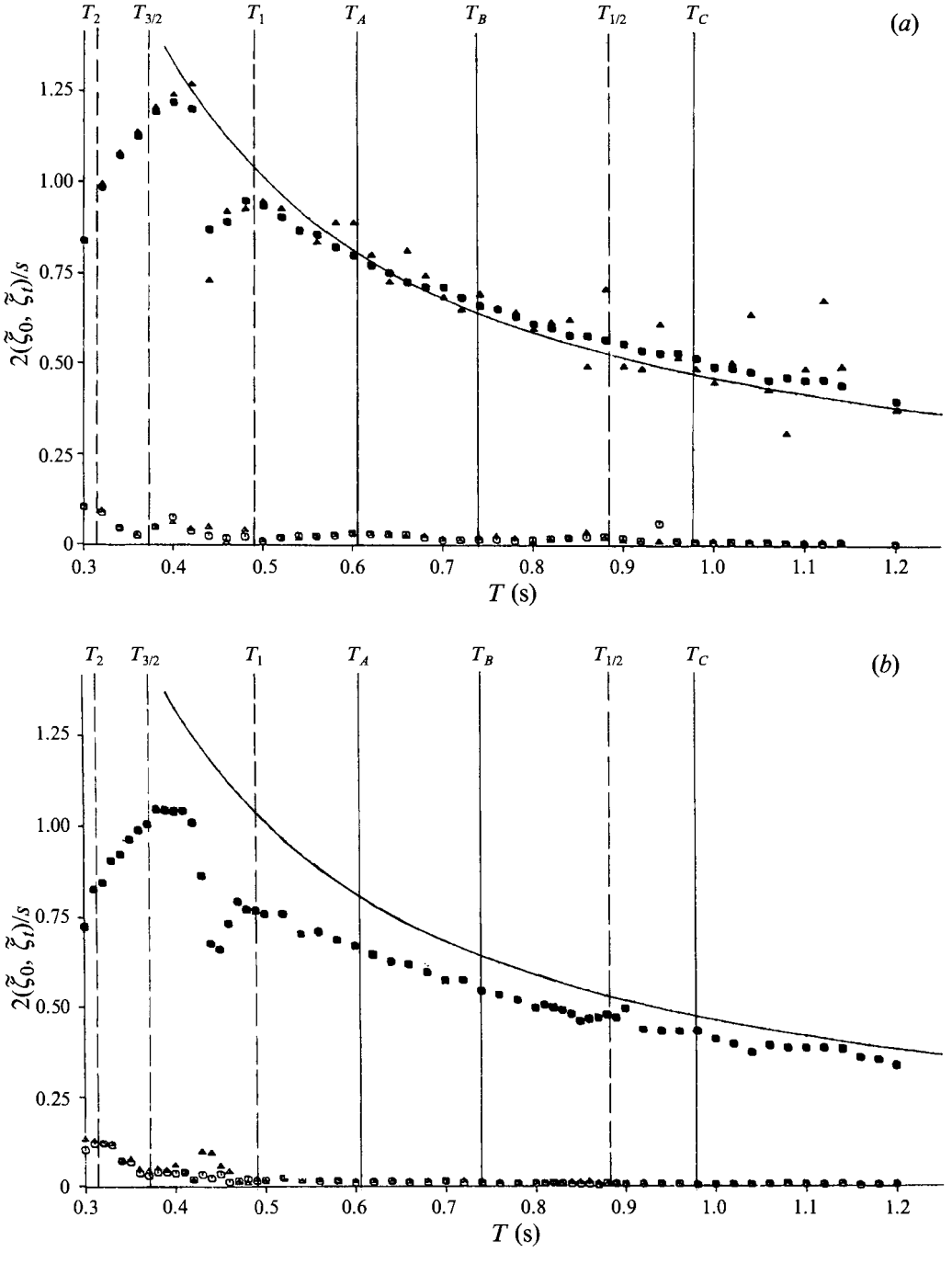

FIGURE 4(*a*, *b*). For caption see facing page.

wave amplitudes; the circular symbols refer to measurements made from the transient wave field and the triangular symbols refer to measurements made from the steady wave field. Measurements of the longitudinal component for the steady wave field are given only in figure 4(*a*). The terminating beach for these experiments had a slope of 5.71°.

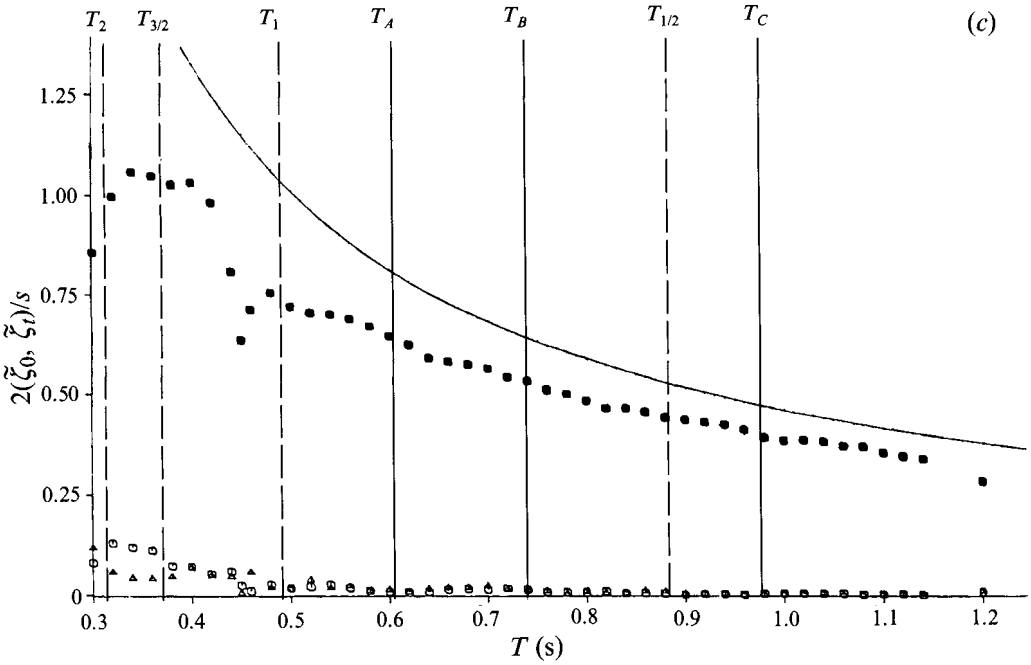

FIGURE 4. Measurements of the wave amplitudes $\tilde{\zeta}_0$ and $\tilde{\zeta}_t$ at $X = 30.0$ as a function of the wavemaker period T. ▲, ● refer respectively to measurements from the longitudinal steady and transient wave fields, and △, ⏀ refer respectively to the transverse steady and transient wave fields. The curve shows the expectation from linear wavemaker theory. The marked periods are: $T_2 = 0.3122$ s, $T_{3/2} = 0.3704$ s, $T_1 = 0.4908$ s, $T_A = 0.6048$ s, $T_B = 0.7376$ s, $T_{1/2} = 0.8828$ s, $T_C = 0.9741$ s. The water depth H was 50.0 mm. (*a*) Wavemaker stroke $s = 0.53$ mm; (*b*) $s = 1.47$ mm; (*c*) $s = 5.06$ mm.

The measurements of the steady-state wave amplitudes at $X = 30.0$ show a considerable degree of variation as a function of T. This derives from imperfect absorption of the incident waves at the beach, so that the steady wave field is a combination of an outward-travelling and a reflected wave train. The partitioning of the wave field into these two components requires more information than just the vertical range of movement of the water surface at a given location, because the relative phases of the waves depends both on the positioning of the beach and on the period T. But this effect would suggest that, by taking averages of $\tilde{\zeta}_0$ locally in the period T, the steady-state amplitudes should give a reasonably good estimate of the incident wave amplitude and, indeed, when interpreted in this way the two sets of data are found to be in broad agreement with each other. (More detailed descriptions of the partitioning of wave measurements of the kind described here are given by Mahony & Pritchard 1980 and by Benjamin, Boczar-Karakiewicz & Pritchard 1987, and further examples of the steady-state field are described below.)

The method by which the estimates of the incident-wave amplitude at $X = 30.0$ were made from the unsteady measurement needs some explanation. Initially the water in the tank was motionless and, at a given instant, the wavemaker was set oscillating with period T. The wave amplitude at $X = 30.0$ was recorded and it was found that, after five or six crests had passed, the wave amplitude was nearly constant and remained so until the wave train reflected from the beach reached the measuring station. (The location of the measuring station was such that there was a good period of time between when the incident wave field was nearly at its steady state and when the

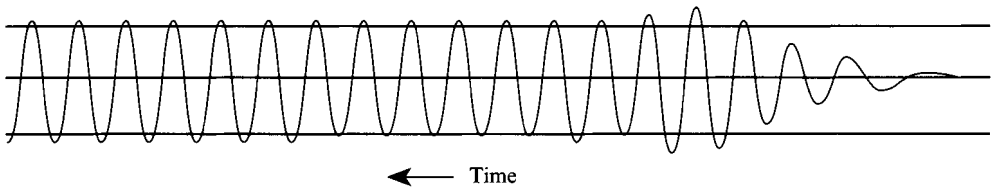

FIGURE 5. A typical example of the temporal development of the longitudinal component of the wave field at $X = 30.0$ in response to the wavemaker suddenly set oscillating with a period $T = 0.4600$ s. The steady peak-to-trough amplitude of this wave was approximately 0.64 mm. The water depth H was 50.0 mm.

reflected wave train had reached the measuring station.) An example of the build-up of the wave train at $T = 0.4600$ s is given in figure 5. In this figure time increases from right to left and we see, at the extreme right, the build up of the wave to maximal surface displacements on the fourth crest and fifth trough, after which the wave field quickly settled into an oscillation of nearly constant amplitude. The same general pattern is also found from numerical calculations made on one of the model equations for the propagation of long waves, the so-called BBM equation (see Benjamin, Bona & Mahony 1972), in which the surface displacement $\zeta(x, t)$ $(:= \tilde{\zeta}_0/H)$ satisfies the equation

$$\zeta_t + \zeta_x + \tfrac{3}{2}\zeta\zeta_x - \mu\zeta_{xx} - \tfrac{1}{6}\zeta_{xxt} = 0, \tag{4}$$

where $x := \tilde{x}/H$ and $t := \tilde{t}(g/H)^{1/2}$. Numerical methods for this model have been developed by Bona, Pritchard & Scott (1980). The model, with an appropriate choice for the constant μ, used to represent dissipative effects, gave very good predictions of a set of laboratory experiments. Equation (4) has been solved for $x, t > 0$, with initial data $\zeta(x, 0) = 0$ and boundary data $\zeta(0, t) = h_0 \sin \omega t$, where the initial wave amplitude h_0 and the frequency ω have been chosen to match the experimental conditions shown in figure 4. The results of the computations are given in the Appendix. From these it is seen that, in the presence of small dissipative effects, the wave field according to (4) does indeed settle down to a nearly periodic state after the first few crests have passed the observation station at $X = 30.0$. (If, on the other hand, there are no dissipative effects it appears from the computations that the wave field at $X = 30.0$ can take a very large time to settle down to a steady amplitude.) An interesting feature of the computations is the importance of nonlinear effects in modifying the sinusoidal waveform, especially at the larger values of T used in the experiments.

It is seen from figure 4(*a*) that the observed wave amplitudes were in quite good agreement with those predicted from linear wavemaker theory, for periods in excess of the period T_1 labelled on the figure. There are, however, two competing effects to be taken into consideration when interpreting these results. On the one hand, no allowance has been made here for dissipation of the waves as they progress along the channel – this would reduce the expected theoretical wave amplitude by about 10% near the mid-range of the periods and by about 5% near the upper end of the range of periods; at the smaller values of T, measurements of the wave field along the channel indicated a reduction of approximately 30% in amplitude between the wavemaker and the station at $X = 30.0$. On the other hand, with the very small wavemaker strokes for figure 4(*a*) there was, especially at the larger periods, a small amount of flexure of the stand on which the measuring device was mounted, and we believe that this resulted in a slight underestimate, of a few percent, of the wavemaker stroke. Thus, in view of such allowances, the experiments depicted in figure 4(*b*), for which the nonlinearity was not of overriding importance (cf. the Appendix), would appear to have been fairly well

represented by the classical wavemaker theory. For the experiments made with larger wavemaker strokes it is apparent, from figure 4(*c*), that the observed response at $X = 30.0$ was modified to a certain extent by nonlinear effects.

An unusual feature evident in all three parts of figure 4 is the dramatic, almost discontinuous change in the value of $\tilde{\zeta}_0$ at a period of approximately 0.43 s. As is apparent from figure 4(*a*), this phenomenon was evident in the measurements from both the transient and the steady measurements of the longitudinal-wave fields. We do not at present have an explanation of this effect.

(Note in review: A referee suggested the possibility of enhanced energy dissipation at the anomalous frequencies arising from an interaction of the surface gravity wave with longitudinal waves of a monolayer contamination at the surface.)

It is seen from figure 4 that the amplitudes of the transverse-wave fields in the channel were nearly the same for both the transient and the steady-state measurements, and that these fields were a small proportion, of the order of 3 or 4%, of the amplitudes of the longitudinal fields. Note that, in the frequency range near $T = 0.43$ s, where the longitudinal field showed an abrupt change in amplitude, there were no apparently anomalous features of the transverse fields.

4.1.2. *The wave field along the channel*

Extensive measurements have been made of the steady-state wave field along the channel. Such measurements are needed to ascertain the magnitudes of the incident and reflected components of the wave field at the toe of the beach. These fields must be found empirically for each operating condition as the amplitude (and phase) of the waves generated by the wavemaker are dependent on the conditions established in the channel; in particular, the wave field must be such that, at steady state, the energy imparted to the wave field by the wavemaker exactly balances the energy dissipation in the channel.

Examples of wave fields observed at a forcing period $T = 0.6064$ s are given in figure 6. The period used for these experiments was a period at which subharmonic generation of edge waves was possible and, indeed, at the three largest wavemaker amplitudes used for the experiments depicted in parts (*c*,), (*d*) and (*e*) of the figure, edge waves were present over the beach. Shown in this figure are the amplitudes of longitudinal-wave fields (measured along the centreline of the channel), as well as the amplitudes of the transverse-wave fields observed in the main part of the channel. There is seen to be a qualitative difference between the transverse-wave fields in parts (*a*) and (*b*) of the figure, compared with those in (*c*), (*d*) and (*e*) when an edge wave was present over the beach.

As described in Benjamin *et al.* (1987), the longitudinal-wave field can be decomposed into incident and reflected components for which the magnitude of the envelope of the oscillations evident in figure 6 indicates the size of the reflected-wave field, and the mean level indicates the amplitude of the incident waves. Thus, we see from the figure that the amplitude of the outward-travelling wave decayed in the direction away from the wavemaker (located at X_W), and the magnitude of the reflected-wave field decayed in the direction from the beach to the wavemaker. From such a partitioning we can estimate the relative amplitudes of the incident and reflected longitudinal-wave fields, an evaluation of which, made near the toe of the beach, provides a measure of the reflection coefficient r from the beach. The values of r relating to the experiments depicted in figure 6 are given in table 1 and it is seen that the reflected-wave amplitude was approximately 50% of that of the wave incident on the beach, except for the two largest forcing levels, under which conditions the reflected wave component was

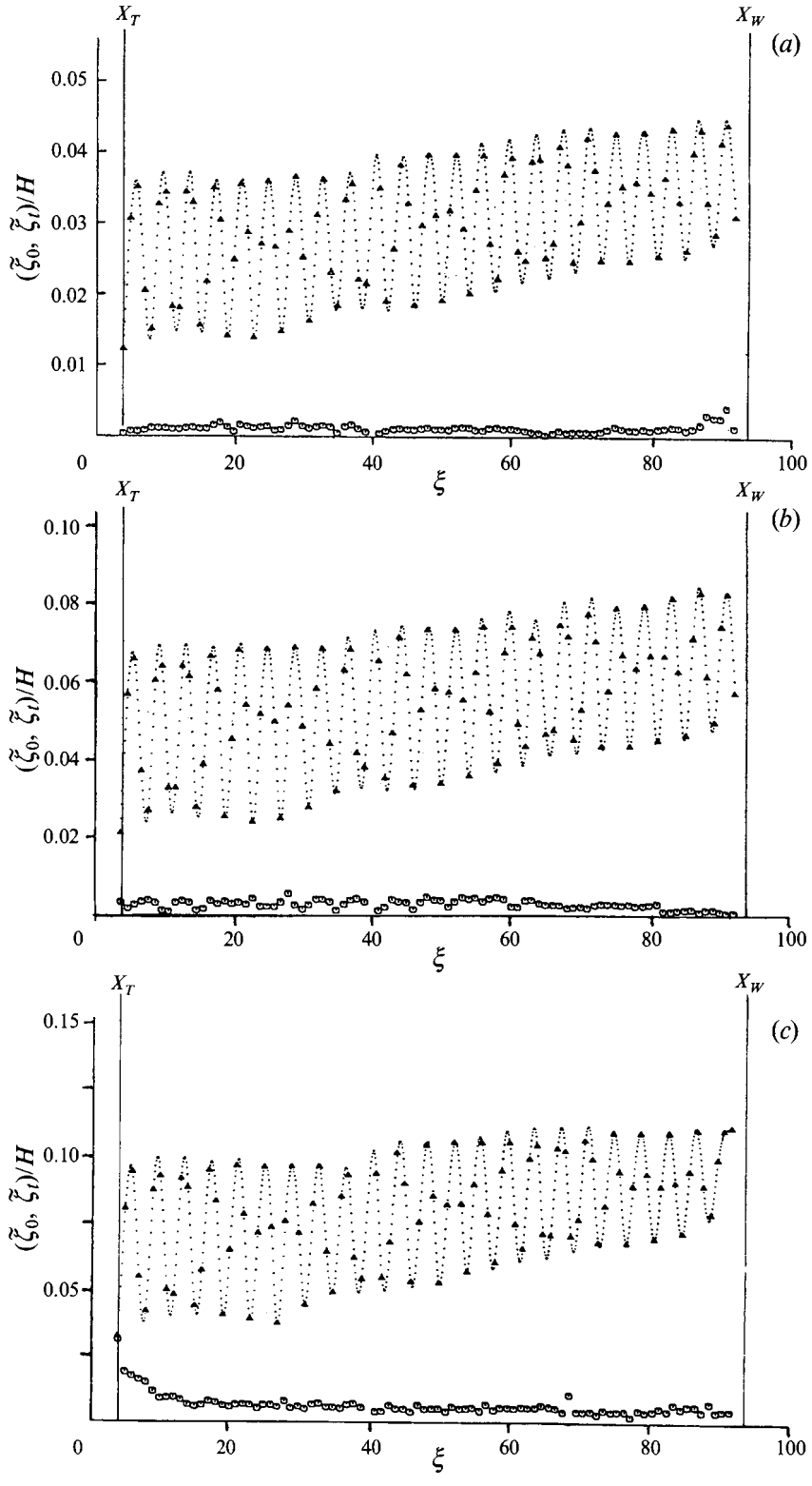

FIGURE 6(*a–c*). For caption see facing page.

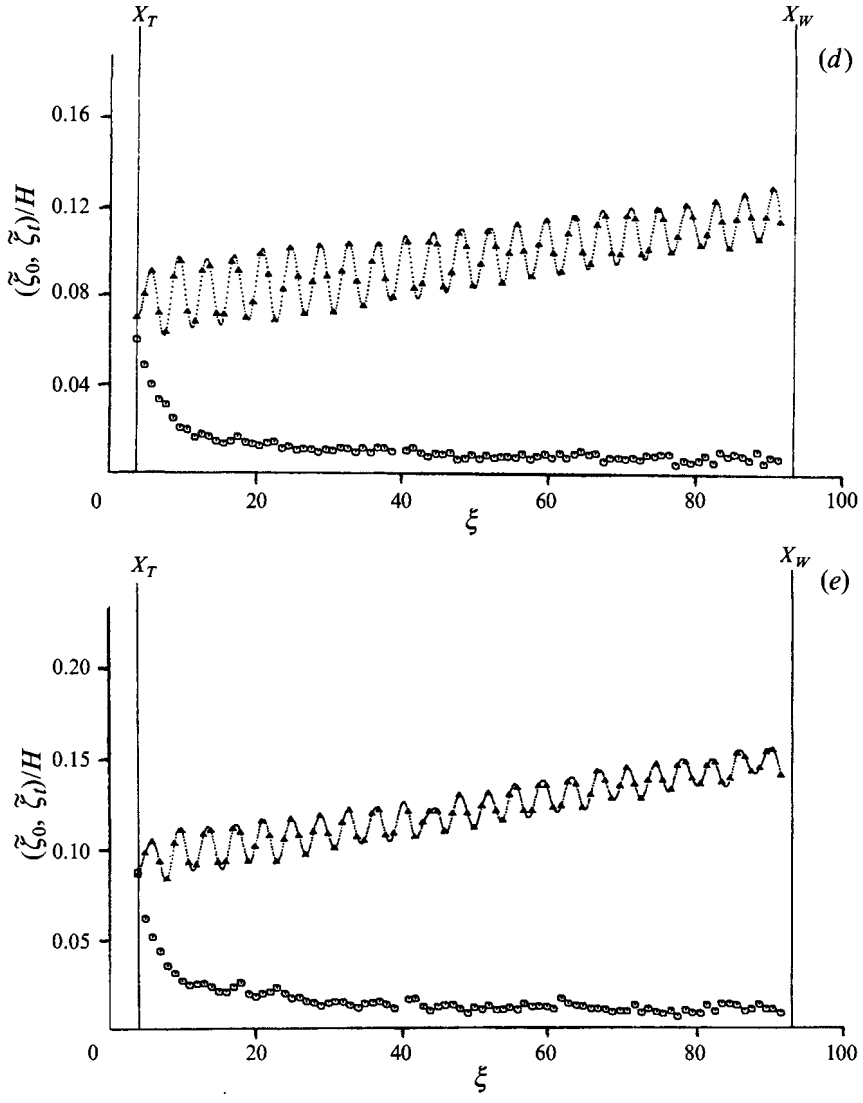

FIGURE 6. Measurements of the steady-state wave amplitudes, $\tilde{\zeta}_0$ and $\tilde{\zeta}_t$ in the uniform section of the channel, at a period $T = 0.6064$ s, for various forcing amplitudes, s, of the wavemaker. Distances $\xi(= (L-\tilde{x})/H)$ along the channel are measured from the location of the shoreline on the beach; X_T denotes the location of the toe of the beach, and X_W is the location of the wavemaker. The depth $H = 50.0$ mm and the beach angle $\beta = 15°$. ▲, ⓣ denote the longitudinal- and transverse-wave fields respectively. (*a*) Stroke $s = 2.0$ mm; (*b*) $s = 4.0$ mm; (*c*) $s = 6.0$ mm; (*d*) $s = 8.0$ mm; (*e*) $s = 10.0$ mm. Note that in experiments (*c*), (*d*) and (*e*) an edge wave was present over the beach.

Stroke s (mm)	2.0	4.0	6.0	8.0	10.0
$r(X_T)$	0.50	0.53	0.50	0.22	0.14
$\mathscr{L}$ (m)	12.7	11.8	11.9	10.6	9.6

TABLE 1. Properties of the wave fields depicted in figure 6. Here r denotes a reflection coefficient, $\mathscr{L}$ is a decay length and X_T denotes the position of the toe of the beach. The slope of the beach for these experiments was 15° and the period $T = 0.6064$ s.

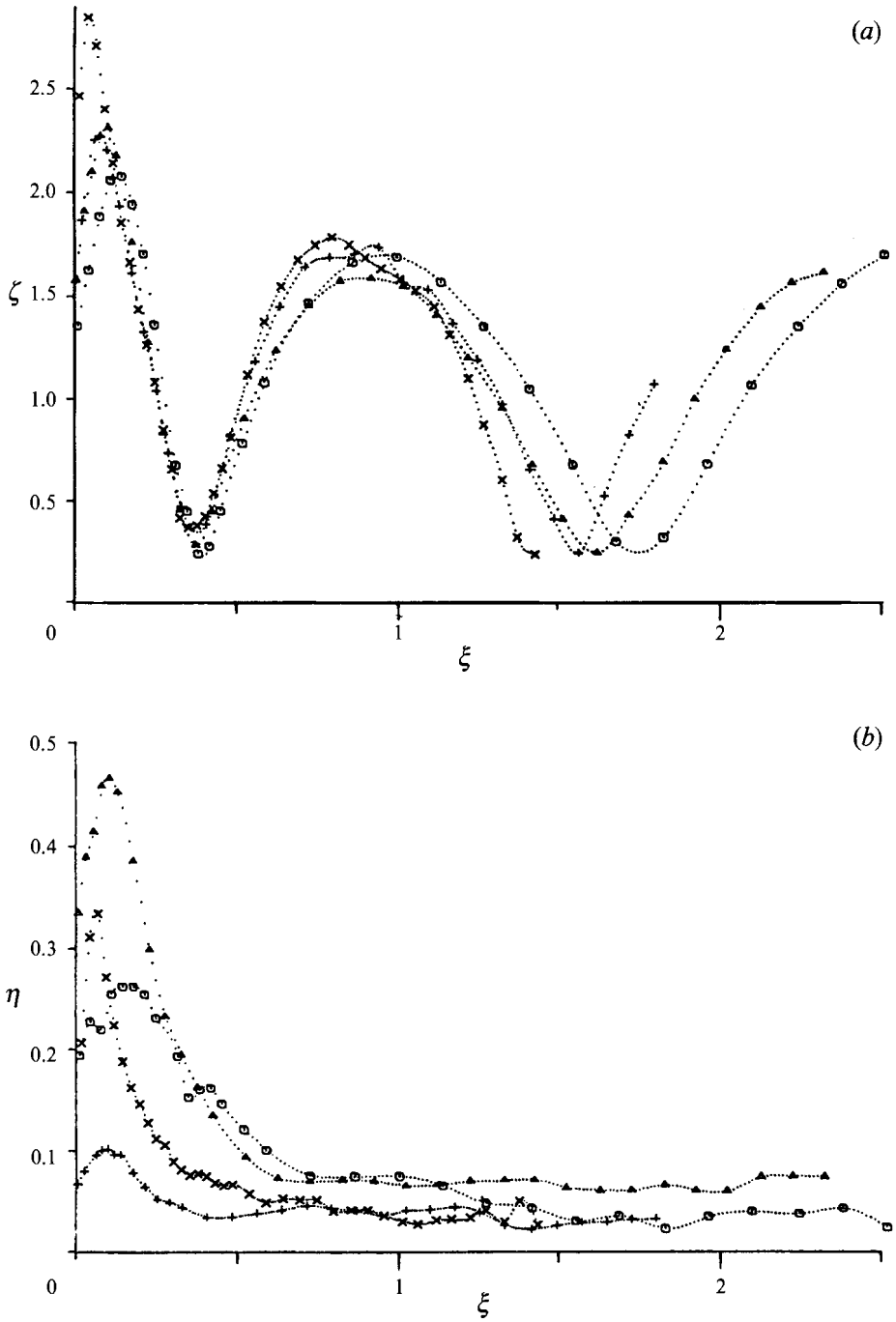

FIGURE 7. The steady (primary) wave field over a beach of slope 15° as a function of distance ξ from the shoreline, for various forcing frequencies and for a wavemaker amplitude $s = 8.0$ mm. (*a*) Longitudinal-wave fields, $\zeta = \tilde{\zeta}_0/\tilde{\zeta}_0(\xi_T)$; (*b*) transverse-wave fields, $\eta = \tilde{\eta}_0/\tilde{\zeta}_0(\xi_T)$, where ξ_T denotes the location of the toe of the beach. Water depth $H = 50.0$ mm. The symbols correspond respectively to the following wavemaker periods, incident-wave amplitude $\tilde{\zeta}_0 (= \tilde{\zeta}_0(\xi_T))$ at the toe of the beach and locations ξ_T of the toe of the beach. ⊙, $T = 0.7500$ s, $\tilde{\zeta}_0 = 2.57$ mm, $\xi_T = 1.29$; ▲, $T = 0.8800$ s, $\tilde{\zeta}_0 = 2.64$ mm, $\xi_T = 0.91$; + $T = 1.0000$ s, $\tilde{\zeta}_0 = 2.90$ mm, $\xi_T = 0.73$; ×, $T = 1.2128$ s, $\tilde{\zeta}_0 = 1.89$ mm, $\xi_T = 0.48$.

considerably smaller. At these larger forcing levels there was a substantial amount of wave breaking near the shoreline of the beach and also the presence of a healthy edge wave over the beach.

It is also possible from the data shown in figure 6 to estimate a (spatial) rate of decay of the outward-travelling waves. Suppose that the amplitude of the outgoing wave field is of the form $\tilde{\zeta}_0(0) \exp(-\tilde{x}/\mathscr{L})$, where $\mathscr{L}$ denotes a lapse rate for the waves. The values of $\mathscr{L}$ relating to the data of figure 6 are also given in table 1, from which it is seen that the lapse rate for these waves was around 10 to 12 m.

The results depicted in figure 6 are typical of the wave fields observed at other frequencies and with different beach slopes. Data of this kind were used to determine the amplitudes of the longitudinal-wave train near the toe of the beach under each operating condition, so that all wave measurements over the beach could be scaled by the size of the incident-wave field at the toe of the beach, determined by the procedure described above. A potentially important property for the generation of edge waves is the magnitude of the reflected-wave field. The measurements for table 1 were made at a frequency at which edge waves were expected to develop over the 15° beach. For comparison, the reflection coefficient at the critical frequency of 0.7400 s for a 10° beach was $r \approx 0.4$, and at the critical frequency of 0.9776 s for the 5.65° beach was also $r \approx 0.4$. Both these latter measurements were for a forcing amplitude at the wavemaker of $s = 2.0$ mm.

4.2. *The wave field over the beach*

Examples of the wave field over the beach are given in figures 7 and 8. The wave amplitudes given here have been normalized with respect to the measured amplitude of the incident wave at the toe of the beach, determined in the manner described above in §4.1.2. (Each of the normalizing amplitudes is quoted in the figure caption.) The results given in figure 7 show the wave field over a beach of slope $\beta = 15°$ at a number of different frequencies, and the data for figure 8 are for a beach of slope $\beta = 10°$ for a fixed wave period, but for a range of different forcing amplitudes.

The ξ-coordinate used in these figures has been scaled by the decay length for the Stokes edge wave (cf. (1) and (2)) so that $\xi := \tilde{\xi}\omega^2/4g \tan\beta$. The factor 4 appearing in this formula assumes that edge waves arising in the experiment have frequency approximately $\frac{1}{2}\omega$. This scaling means that, for figure 7, the toe of the beach is located at different values of ξ for each of the frequencies: the actual locations are given in the figure captions. Under such a scaling it is seen (figure 7*a*) that the longitudinal-wave fields over the beach had similar amplitude distributions: moving away from the shoreline the amplitude increased to a maximum value of roughly two and a half times the incident-wave amplitude, and then decreased to a local minimum of roughly 0.3 times the incident-wave amplitude. These results are in keeping with the measurements reported by Mahony & Pritchard (1980) in which it was suggested that frictional effects on the beach had a strong influence on the character of the wave field. In particular, the sharp reduction in wave amplitude near the shoreline, as evidenced in all the measurements of both the longitudinal- and the transverse-wave fields, is characteristic of the property that viscous dissipation was a significant factor in the zone near the shoreline (cf. Mahony & Pritchard 1980; Miles 1990*b*). In addition to viscous effects playing an important role in the wave dynamics near the shore, there was also clear evidence of wave breaking at the larger amplitudes. This usually took the form of capillary ripples developing ahead of the wave crest as it advanced up the beach but, in some of the extreme cases, tumbling breakers were observed. The importance of wave amplitude on the dissipative process can be seen in figure 8 where the size of the local maximum in the wave amplitude nearest the shoreline decreased substantially as

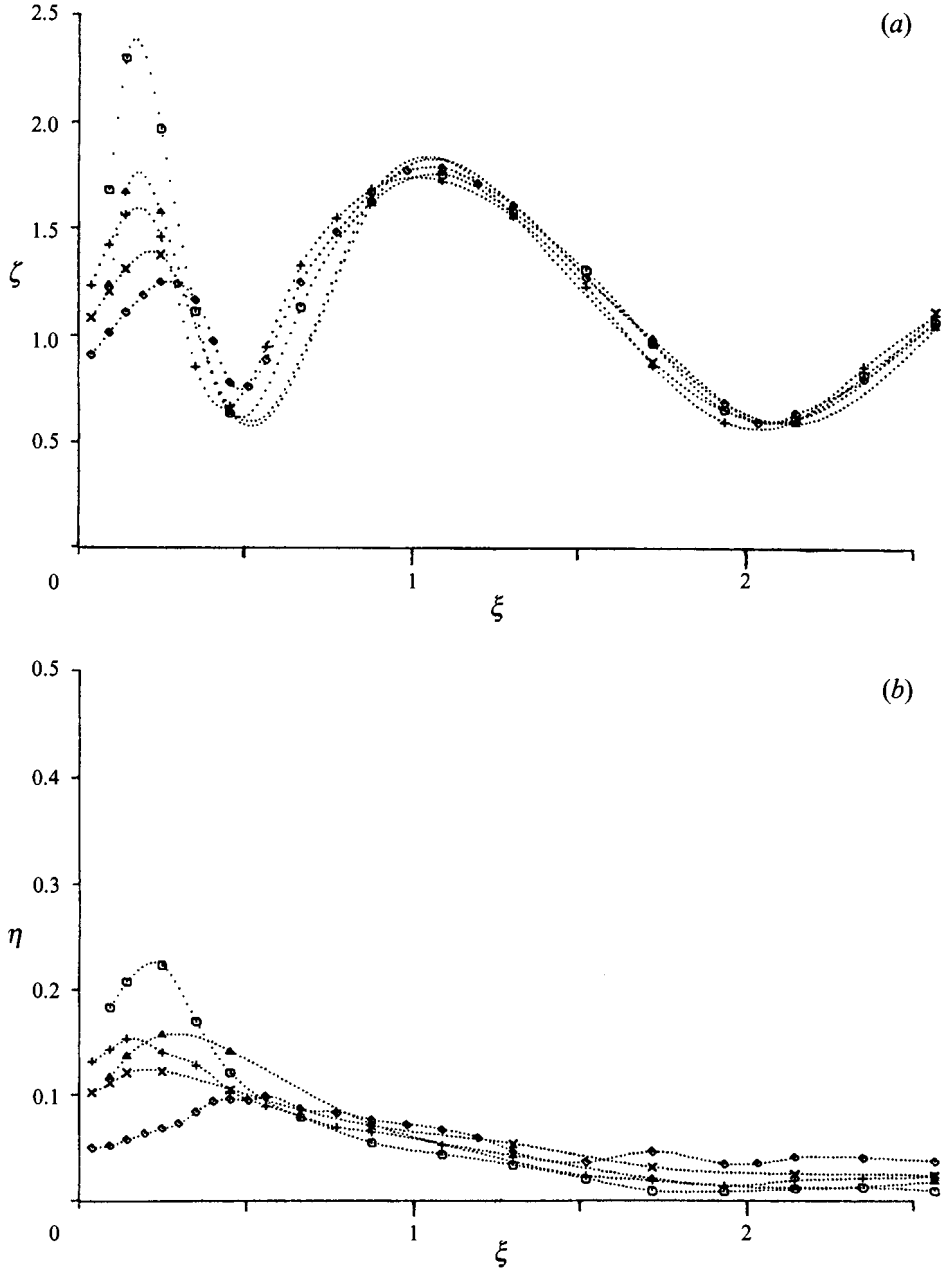

FIGURE 8. The steady wavefield over a beach of slope 10° as a function of distance ξ from the shoreline, at a forcing period $T = 0.7400$ s and for various wavemaker strokes, s. (*a*) Longitudinal-wave fields, $\zeta = \tilde{\zeta}_0/\tilde{\zeta}_0(\xi_T)$; (*b*) transverse-wave fields, $\eta = \tilde{\eta}_0/\tilde{\zeta}_0(\xi_T)$, where ξ_T denotes the location of the toe of the beach. Water depth $H = 50.0$ mm. The toe of the beach is at $\xi = 2.95$. The symbols correspond respectively to the following values of s and to the incident wave amplitude $\tilde{\zeta}_0 (= \tilde{\zeta}_0(\xi_T))$ at the toe of the beach. ⊙, $s = 2.0$ mm, $\tilde{\zeta}_0 = 0.74$ mm; ▲, $s = 4.0$ mm, $\tilde{\zeta}_0 = 1.40$ mm; +, $s = 6.0$ mm, $\tilde{\zeta}_0 = 2.21$ mm; ×, $s = 8.0$ mm, $\tilde{\zeta}_0 = 2.91$ mm; ◇, $s = 10.0$ mm, $\tilde{\zeta}_0 = 3.40$ mm.

the amplitude of the forcing was increased. Also, it is seen that the location of the local maximum in wave amplitude nearest the shoreline was strongly dependent on the wave amplitude. Thus, the waves of largest incident amplitude were the ones most strongly attenuated near the shore and their near-shore local maximum occurred furthest from the shore line.

It is seen in figure 7(*a*) that, at the smallest wave frequency (corresponding to $T = 1.2128$ s) the relative maximum wave amplitude near the shore was considerably larger than that which obtained at the other frequencies, a consequence (presumably) of the smaller influence of viscous effects at the smaller frequencies. The transverse-wave fields shown in figure 7(*b*) are of interest in that the forcing periods T of 0.8800 s and 1.2128 s correspond respectively to natural frequencies for a full- and a half-wavelength transverse mode, and it is seen that the responses of the transverse-wave fields were indeed enhanced at these frequencies. It will be shown in §6 how imperfections in the beach can lead to very large transverse-wave fields when forced at these natural frequencies. We shall, on the other hand, see that edge waves generated parametrically, by a subharmonic instability, are far more vigorous than the modes shown here.

5. The edge-wave field

Series of experiments were made with beach slopes of 5.71°, 10.0° and 15.0° to try to generate edge waves over these beaches by a subharmonic interaction mechanism. (Attempts to generate the edge-wave modes synchronously are described in §6.) The resonant forcing frequency (2σ) for the 5.71° beach had the period labelled T_C in figure 4: all attempts made at this, and neighbouring periods, to generate edge waves proved unsuccessful, even at the largest forcing amplitude of 10 mm stroke available with the wavemaker. Indeed, at this level of forcing, the incident waves were so large in amplitude that breaking, in the form of capillary ripples between the wave crests, occurred just in front of the wavemaker.

The resonant forcing frequency for edge waves over the 10.0° beach had the period labelled T_B in figure 4. As with the 5.71° beach, no edge waves appeared spontaneously at any forcing amplitude up to a stroke of 10 mm. However, at the larger strokes of 9 or 10 mm, stable edge waves could be generated by making a sufficiently large disturbance to the water surface near the shoreline, usually achieved by blowing across the surface. On the other hand, it was found that edge waves formed spontaneously over the 15° beach at the larger wavemaker strokes when the wavemaker period was near the potentially resonant value T_A (cf. figure 4). Photographs of edge waves over the 15° beach are shown in figure 9, from which it is seen just how effective, even violent, the subharmonic resonance effect can be in driving wave motions. So, for example, at the relatively small wavemaker stroke of 4.0 mm, the maximum excursion of the shoreline of the edge wave was approximately 110 mm and, at the larger forcing amplitude shown in figure 9, the run-up of the edge wave was approximately 200 mm. The capillary ripples, so clearly evident in figure 9(*b*), are manifestations of wave breaking, which was prevalent at the larger forcing amplitudes over the 15° beach. An interesting feature of the motions was that, relative to the equilibrium shoreline, the backwash of the waves was only of the order of 10 to 20 mm, even in the extreme case shown in figure 9(*b*). The fact that the backwash of the waves was so small enabled us to make measurements of the edge-wave amplitudes closer to the equilibrium shoreline than might have been imagined. Such measurements were also helped by being able to use the smaller of the capacitance transducers for all but the very largest waves.

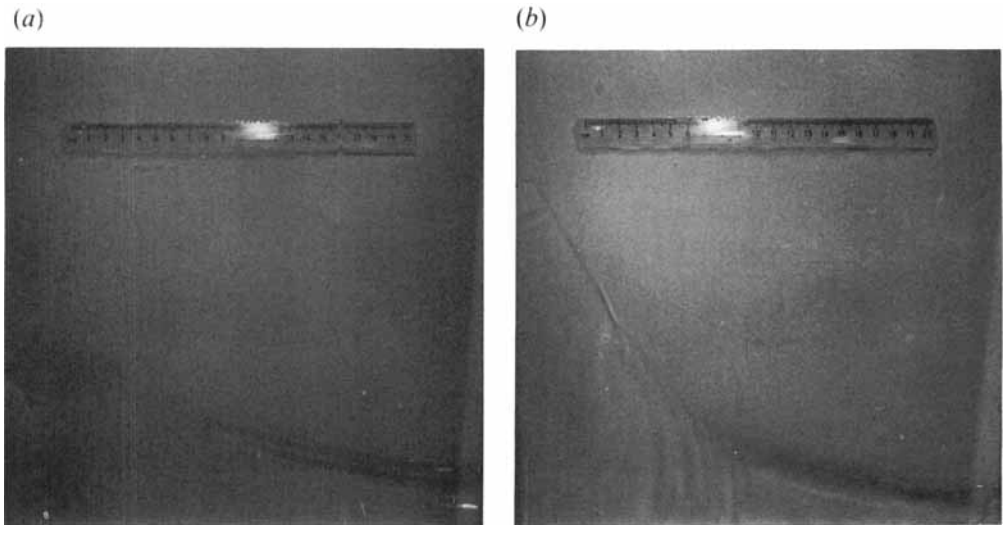

FIGURE 9. Photographs of edge waves over a 15° beach formed at a forcing period T of 0.6064 s. (*a*) Wavemaker stroke $s = 4.0$ mm; (*b*) $s = 8.0$ mm. Water depth $H = 50.0$ mm. The photographs are snapshots of the shoreline at the time of maximum excursion, seen near the left-hand wall, and some capillary ripples associated with the wave motion can also be seen. Also evident is a curve, which delineates the maximum wash of the wave up the beach, and is the edge of a thin film of water left on the beach after the wave recedes. The scale shown in the photographs is in cm.

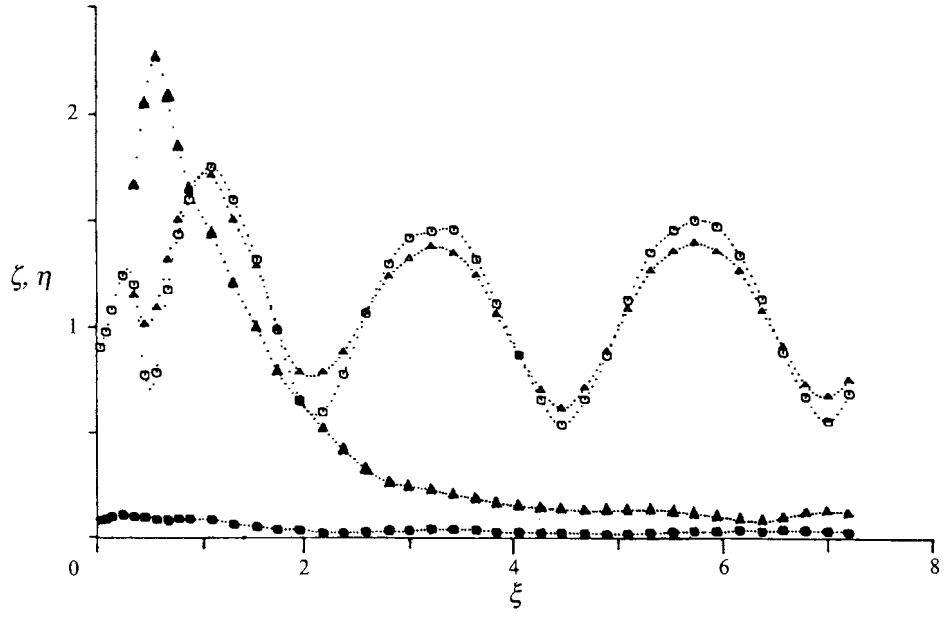

FIGURE 10. Longitudinal- and transverse-wave fields over a 10° beach at a forcing period $T =$ 0.7400 s, with an undisturbed water depth of 50.0 mm. Wavemaker stroke $s = 9.0$ mm. The toe of the beach was at $\xi = 2.95$. ⊙, ▲, longitudinal-wave fields $\zeta = \tilde{\zeta}_0/\tilde{\zeta}_0(X_T)$; ●, ▲, transverse-wave fields $\eta = \tilde{\eta}_0/\tilde{\zeta}_0(X_T)$. For the fields denoted ⊙, ● there was no edge wave present; $\tilde{\zeta}_0(X_T = 3.25$ mm; for ▲, ▲ an edge wave was present; $\tilde{\zeta}_0(X_T) = 3.36$ mm.

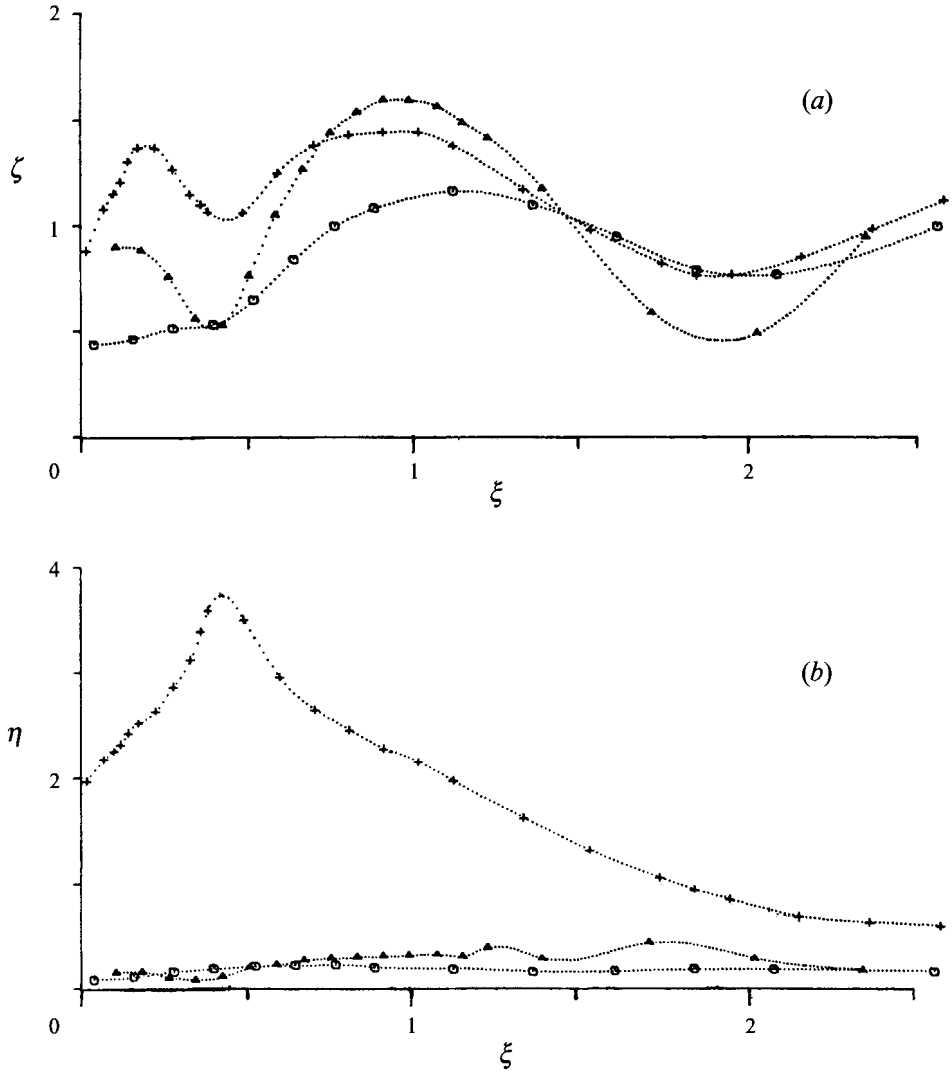

FIGURE 11. Wavefields over a 15° beach at various forcing periods and a wavemaker stroke s = 8.0 mm, with an undisturbed water depth H = 50.0 mm. (*a*) Longitudinal-wave field; (*b*) transverse-wave field. ⊙, $T = 0.4000$ s; $\tilde{\zeta}_0(X_T) = 6.00$ mm, $X_T = 4.38$; ▲, $T = 0.4900$ s, $\tilde{\zeta}_0(X_T) = 3.45$ mm, $X_T = 2.93$; +, $T = 0.6064$ s, $\tilde{\zeta}_0(X_T) = 3.91$ mm, $X_T = 1.90$.

Measurements comparing the longitudinal- and transverse-wave fields over a 10° beach, with and without an edge wave present, are given in figure 10. As indicated above, the hysteresis associated with the edge wave allowed a measurement of this kind, when the forcing amplitude was not too large. The results indicate a large difference between the background transverse motion and the edge-wave field, whereas the differences between the longitudinal-wave fields, in the presence and absence of the edge wave, were not very pronounced at all. Two aspects of the edge-wave structure deserve special mention. The first is the presence of a maximum wave amplitude occurring at a considerable distance from the shoreline, in contrast to what is expected on the basis of the current edge-wave theories. This phenomenon is common to all the measurements we have made and is believed to be associated with viscous, and possibly

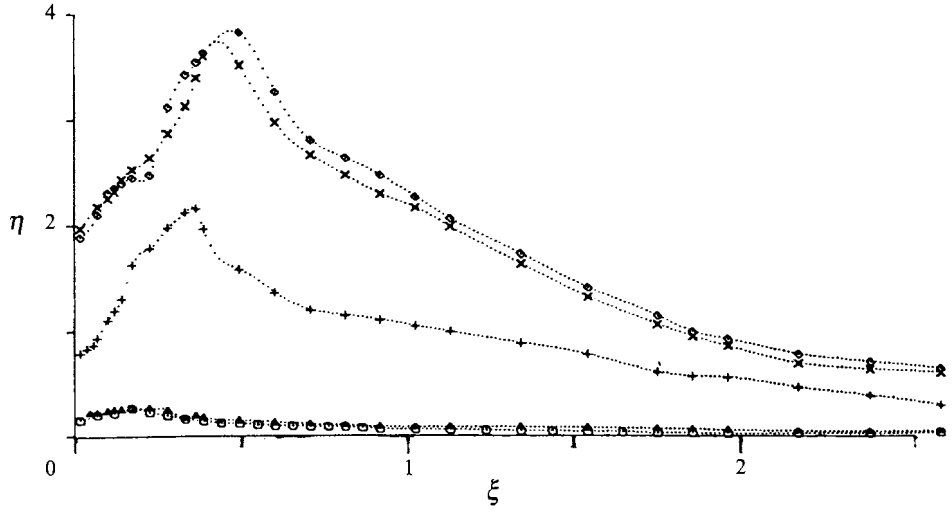

FIGURE 12. Transverse-wave fields over a 15° beach at a forcing period $T = 0.6064$ s, for a variety of wavemaker strokes, s. Water depth $H = 50.0$ mm; $X_T = 1.90$. ⊙, $s = 2.0$ mm, $\tilde{\zeta}_0(X_T) = 1.13$ mm; ▲, $s = 4.0$ mm, $\tilde{\zeta}_0(X_T) = 2.40$ mm; +, $s = 6.0$ mm, $\tilde{\zeta}_0(X_T) = 3.16$ mm; ×, $s = 8.0$ mm, $\tilde{\zeta}_0(X_T) = 3.91$ mm; ◇, $s = 10.0$ mm, $\tilde{\zeta}_0(X_T) = 4.66$ mm.

nonlinear, effects. The second feature of note is the radiation of the edge wave into the uniform section of the channel, ensuring a substantially larger transverse-wave field in the channel than was present before the edge wave was generated. The decay properties of the edge-wave field with ξ will be considered in more detail below.

Examples of the edge-wave and longitudinal-wave fields over a 15° beach are given in figure 11 at two non-resonant frequencies and at the potentially dangerous period T_A. (The wave fields in the uniform part of the channel at the forcing period $T = 0.6064$ s have already been given in figure 6(*e*), to which reference should be made.) Shown in figure 12 are examples of edge-wave fields over the 15° beach at a variety of forcing amplitudes of the wavemaker with the forcing frequency held constant.

The classical theories of Stokes and Ursell indicate that the edge-wave amplitude decreases exponentially with offshore distance, as indicated by (1) and (2). We have compared decay rates of the edge-wave amplitudes (for distances beyond the point where the maximum amplitude was attained) with the theoretical decay rates for the Stokes mode. The result of such a comparison, for the wave depicted in figure 11(*b*) is shown in figure 13, where $\log \eta$ has been plotted as a function of ξ. Also shown in this figure is a linear regression line of best fit of the data, the slope of which is -0.941, not far off the theoretically expected value of -1. Similar comparison have been made with the other edge-wave modes shown in figures 10 and 12. In all these cases regression slopes of approximately -0.9 were obtained (with the exception of the data set at $s = 6.0$ mm of figure 12, which seemed to exhibit a curious kind of bimodal structure) indicating fairly good general agreement with the expected edge-wave decay rate, even if slightly below the theoretical value for the Stokes wave.

5.1. *Margin of stability*

Some experiments were conducted to determine, as a function of frequency, the amplitude of the incident-wave train above which edge waves were sustainable. Such measurements are complicated somewhat by the hysteresis associated with the formation of the edge wave, in that often the initial seeding of the instability had to be

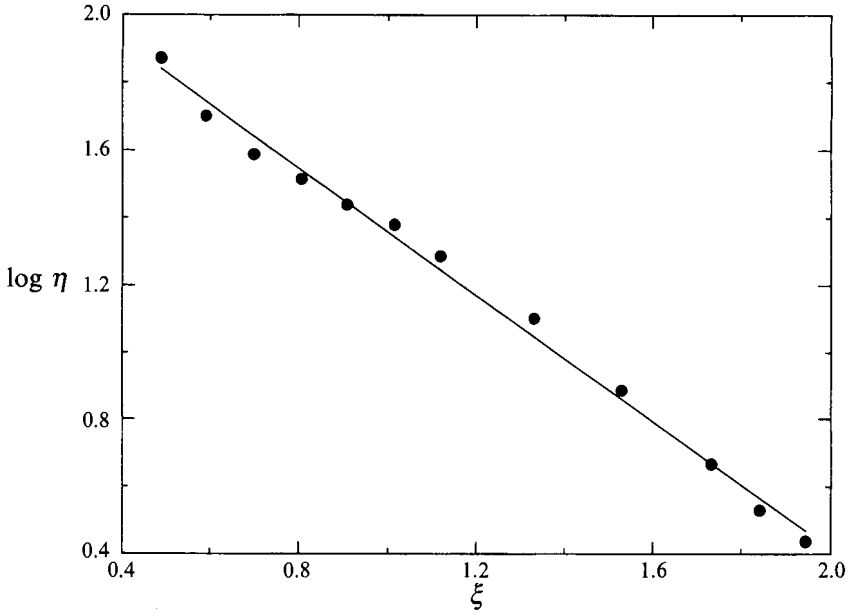

FIGURE 13. The decay rates of the edge wave depicted in figures 11, showing log η as a function of ξ. The straight line is the linear regression curve of best fit to the data and has slope -0.941.

supplied externally, usually by blowing gently on the water surface near the shoreline. Thus, the experimental procedure consisted of establishing a progressive wave field, then carefully perturbing the free surface and watching to see if the resulting disturbance developed into a stable edge wave or decayed, leaving only the progressive field. By using considerable patience, this procedure seemed to be fairly reliable. Moreover, as we shall report below, the present measurements are reinforced by measurements of the initial growth rates of the instability. For the measurements described below the pair of wave transducers used to detect the edge-wave amplitude were located at a distance of 137 mm from the equilibrium shoreline on the beach.

The marginal stability measurements were found to be quite sensitive to small effects. One particularly important quantity was the cleanliness of the free surface. The surface was normally skimmed clean before each measurement but, if the surface was allowed to establish a contaminating film over a period of the order of an hour, it was found that the stability properties were substantially affected. Thus, the shape of the marginal stability curve was not substantially altered, but considerably larger forcing levels were needed to sustain the edge wave.

Measurements of the marginal stability curve for waves over a 15° beach are shown in figure 14(*a*). The curve shows the critical amplitude, ζ_c, of the incident-wave field at the toe of the beach (above which amplitude edge waves were sustained indefinitely) as a function of the forcing period T for the incident-wave train. Note that the curves shown in figure 14 are simply a spline fit of the points. Because of the unexpected nature of the marginal-stability curve in figure 14(*a*), measurements were repeated at a second, quite distinct, water level, the results of which are given in figure 14(*b*). It is seen that the two graphs shown in figures 14(*a*) and 14(*b*) have the same general appearance, even though the precise details differ a little between the two. It is believed, as we shall explain below, that the two local maxima apparent in the marginal stability curves derived from a nonlinear wave interaction associated with the newly formed

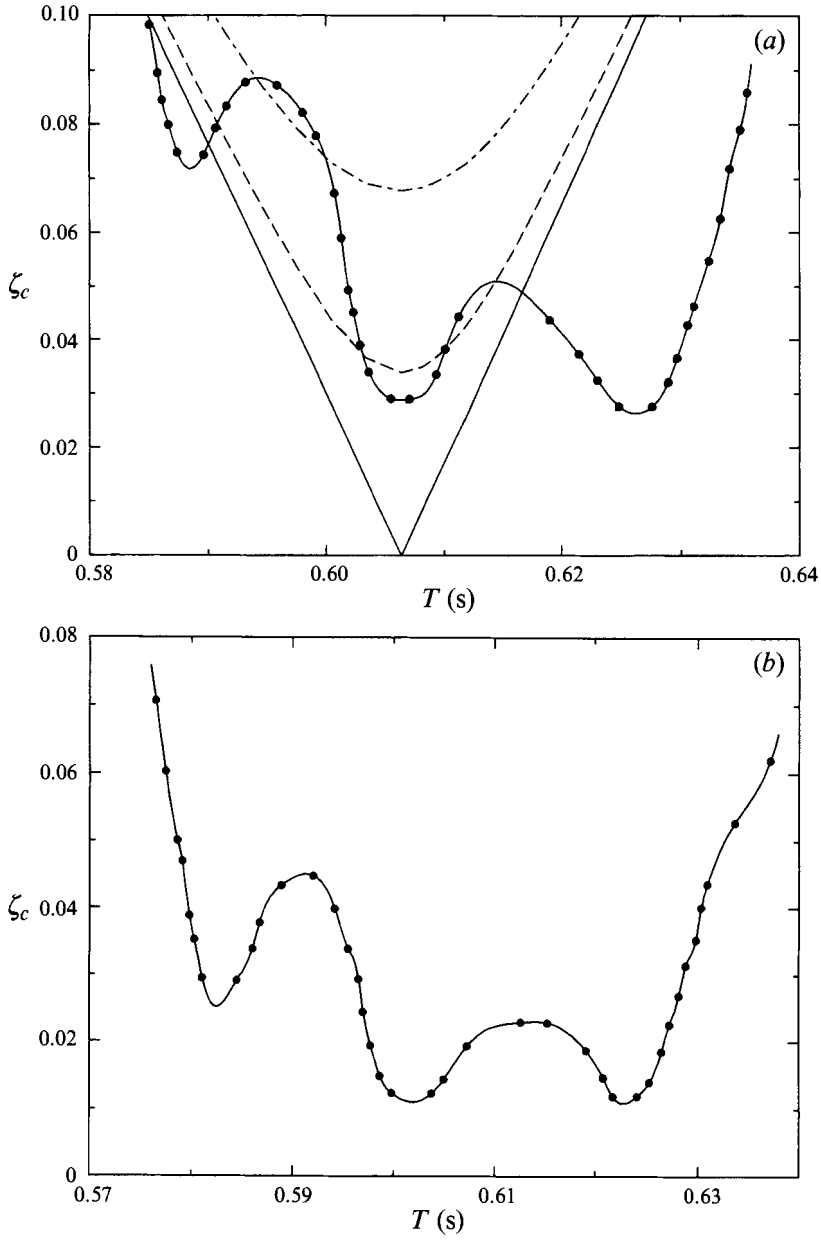

FIGURE 14. Curves of marginal stability for the formation of edge waves over a beach of slope 15°. For a given wavemaker period T, edge waves persisted if the incident-wave amplitude ζ_0/H at the toe of the beach exceeded ζ_c. The experimental points are linked by a spline interpolant. (*a*) Water depth $H = 50$ mm. The theoretical curves correspond to the theory of Miles (1990*a*) and have $C = 0$ (——), $C = 1$ (– – –) and $C = 2$ (–·–). (*b*) $H = 100$ mm.

edge wave. Also shown in figure 14(*a*) are some curves giving the theoretical margin of stability predicted by the theory of Miles (1990*a*). For these calculations the most unstable mode was taken to have arisen at a forcing period of 0.6068 s (edge-wave period 1.2136 s), and the three theoretical curves correspond to damping coefficients $C = 0, 1, 2$ (where C is as given by Miles 1990*a*, p. 55, equation (7.3)), with $C = 1$ for a

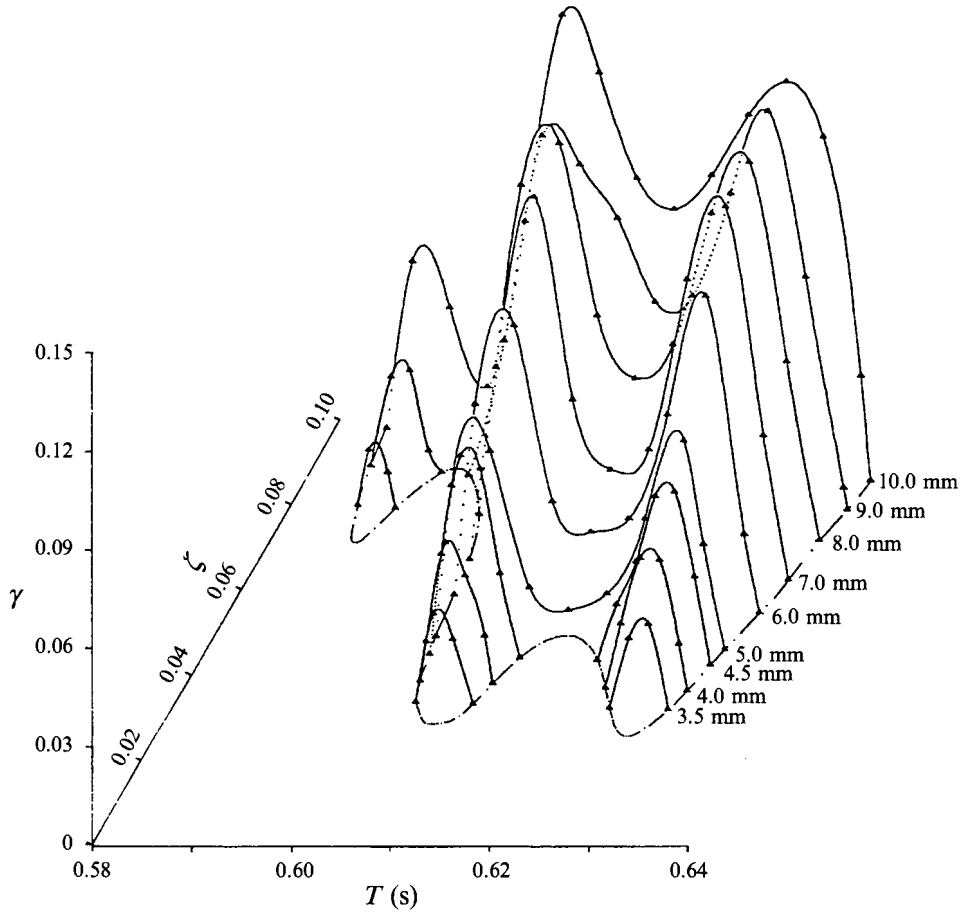

FIGURE 15. Growth rates γ for edge waves over the 15° beach with a water depth $H = 50.0$ mm, for various forcing strokes of the wavemaker (as indicated). Here $\zeta = \tilde{\xi}_0/H$ denotes the incident-wave amplitude at the toe of the beach and T is the wavemaker period. The data points are linked by spline interpolants.

clean surface and $C = 2$ for a fully contaminated surface. The theoretical curves shown in figure 14(*a*) also allow for imperfect reflection of the incident wave, which feature has the effect of broadening, by about 30%, the range of frequencies for which the edge-wave instability was observed. It is seen that, under these conditions, the theoretical bandwidth of the stability boundary is considerably smaller than that observed experimentally, though the presence of another resonant wave mode could account for a further broadening of the stability boundary.

5.2. *Growth rates*

Estimates have been made of the initial rate of growth, γ, of edge waves established in the course of determining the stability boundary shown in figure 14(*a*). To make such estimates it is assumed that the edge-wave amplitude, η, at a given position ξ_0 and during the early stages of its development, can be represented in the form

$$\eta(\xi_0, t) = \eta_i \, \mathrm{e}^{\gamma t},$$

where η_i is some constant. Because of the sensitivity of the capacitance probes used to

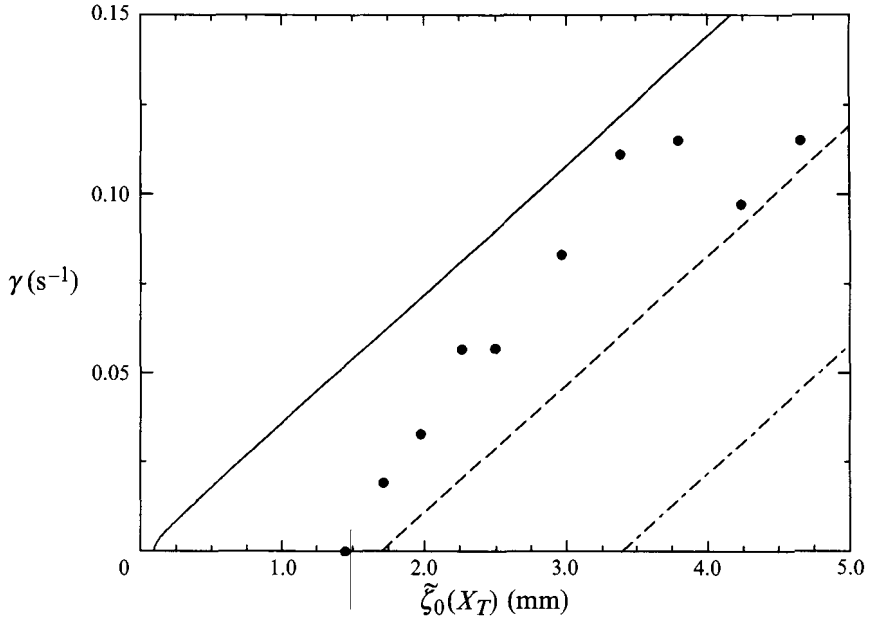

FIGURE 16. Edge-wave growth rates, γ, measured at $T = 0.6068$ s as a function of incident-wave amplitude, $\tilde{\zeta}_0(X_T)$, are compared with theoretical predictions from Miles (1990*a*): ——, $C = 0$; – – –, $C = 1$; – · –, $C = 2$.

measure the wave amplitudes, it was possible to make quite an accurate estimate of γ while the edge-wave amplitudes were still only a small fraction (less than 10%) of the eventual wave amplitude.

The values of γ thus determined are shown in figure 15 for various indicated values of the stroke of the wavemaker. The curve in the plane $\gamma = 0$ is the same as that given in figure 14(*a*). It is seen from the figure that the initial growth rates reflect the same kind of structure as found for the marginal-stability curve, in that there were valleys of small growth rates near the forcing periods of 0.595 s and 0.615 s, at which periods the marginal-stability curve indicates it was relatively difficult to generate the edge waves.

A comparison of the measured values of γ made at $T = 0.6068$ s (namely the values of γ given by the appropriate section of the graph shown in figure 15) has been made with the predicted growth rates given by the theory of Miles (1990*a*, p. 55) and the results are given in figure 16. It is seen from this comparison (in which account was taken of the reflected-wave field observed experimentally) that the theoretical values for $C = 1$ considerably underestimated the measured growth rates of the instability. (We do not have complete confidence in the veracity of the data point at the second largest forcing amplitude, cf. also figure 15, but there was no cogent reason to discard it from the data set.)

In these experiments it was found that, by and large, the edge-wave field eventually settled down to a steady state though, as we shall show below in figure 19, there was a small modulation of the edge-wave field at certain frequencies. A perspective picture of the wave-field amplitudes thus observed is given in figure 17: for the purposes of making this graph we have taken an average value of the edge-wave field when modulation was observed. There is some ambiguity in how to specify the maximum value of the edge-wave amplitude from measurements made at a fixed location

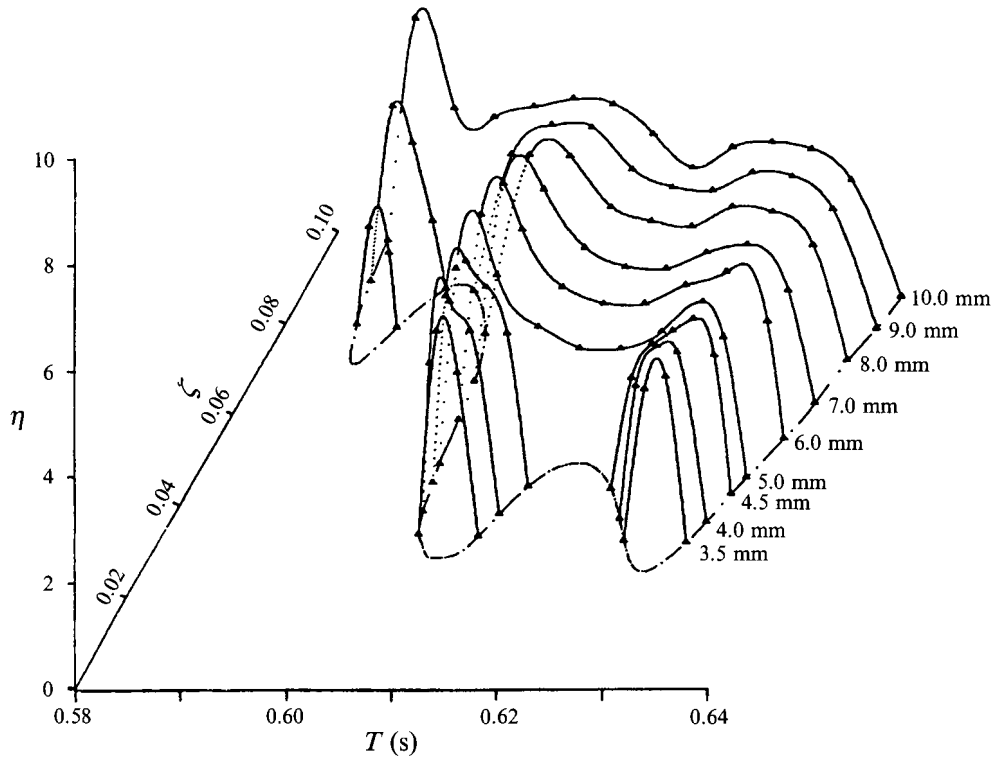

FIGURE 17. Equilibrium values $\eta = \tilde{\eta}/\tilde{\zeta}_0(X_T)$ for the maximum edge-wave amplitude over the 15° beach with a water depth $H = 50.0$ mm, for various forcing strokes of the wavemaker (as indicated). Here $\zeta = \tilde{\zeta}_0/H$ denotes the incident-wave amplitude at the toe of the beach and T is the wavemaker period. The data points are linked by spline interpolants.

(137 mm) offshore. Measurements of the wave amplitude across the channel at this station indicated that it conformed closely to a half-cosine profile, as expected theoretically. Thus, the maximum wave amplitude (at the wall of the channel) at position 137 mm offshore could readily be inferred from the amplitude measured at the offset transducer (cf. §3.4). The maximum wave amplitude, as a function of offshore distance, was less clearly definable, as indicated by the results shown in figure 12, for example. However, from examination of such data it was decided that a constant scaling factor of 2.5 gave a reasonably good estimate of the maximum amplitude compared with that measured at $\tilde{\xi} = 137$ mm. A graph of the maximum edge-wave amplitudes thus estimated, for a forcing period $T = 0.6068$ s is given in figure 18.

5.3. *A tank seiche*

The unexpected nature of the marginal-stability curves shown in figure 14 and of the growth-rate data shown in figure 15 seems to have been associated with a seiching motion in the channel, apparent over a small range of forcing periods above and below the most unstable forcing period for edge waves.

For the experiment depicted in figure 14 the seiche was clearly evident for forcing periods in the approximate intervals [0.5960, 0.6040] s and [0.6160, 0.6240] s, and for respective wavemaker strokes in excess of 7 mm and 4.5 mm. The seiche was found to have a period of approximately 22 times that of the incident wave, as can readily be seen from the modulated incident-wave field shown in figure 19. (Also evident in the

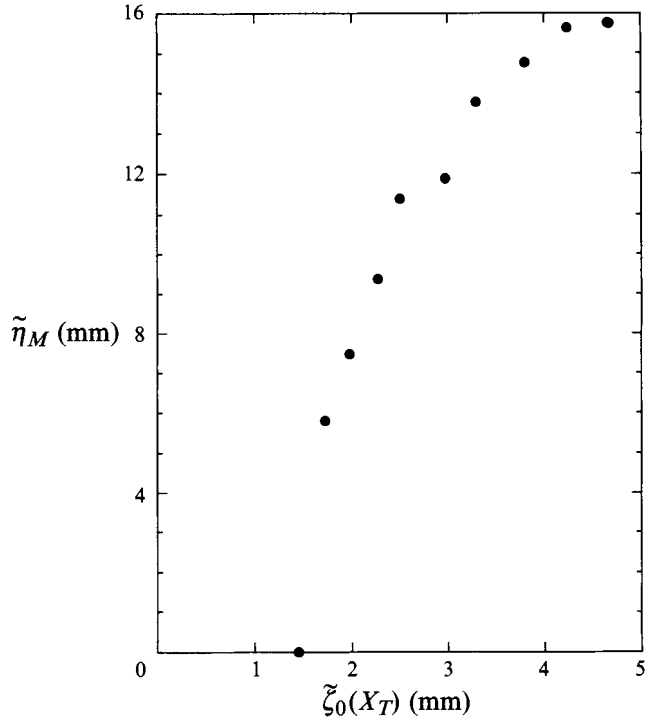

FIGURE 18. The maximum edge-wave amplitude $\tilde{\eta}_M$, as a function of the incident-wave amplitude at the toe of the beach, for $T = 0.6068$ s.

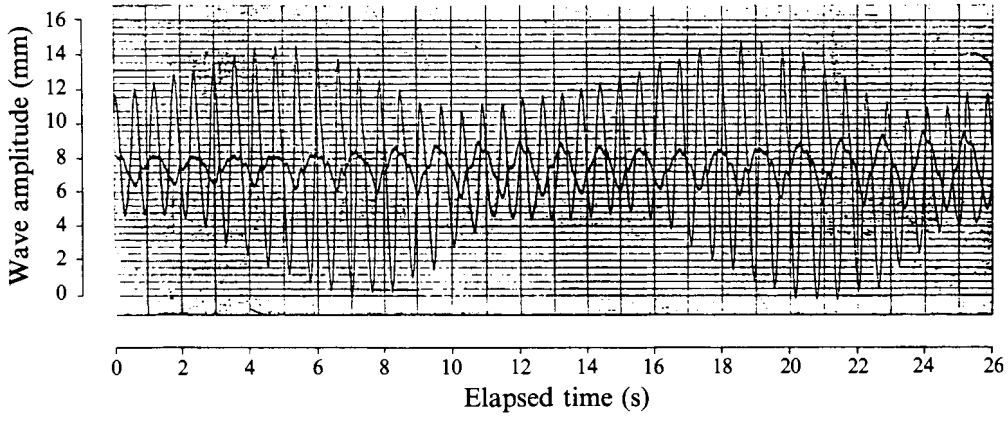

FIGURE 19. Sample record taken during growth-rate measurements. Shown is the modulated longitudinal-wave field and the subharmonic edge wave (central curve) at $\tilde{\xi} = 137$ mm. The amplitude of the edge-wave field has been magnified by a factor of 2. $\beta = 15°$, $s = 9$ mm, $H = 50$ mm, $T = 0.6000$ s.

wave records shown here is a small modulation of the edge-wave field.) The amplitude of the seiching motion was of the same order of magnitude as that of the incident wave for wavemaker strokes in excess of 6 mm, but was of a smaller order for smaller strokes.

Corresponding to forcing frequencies of 0.6000 s and 0.6200 s, the periods of the seiche were 13.20 s and 13.64 s respectively, implying respective wavelengths of 9.22 m

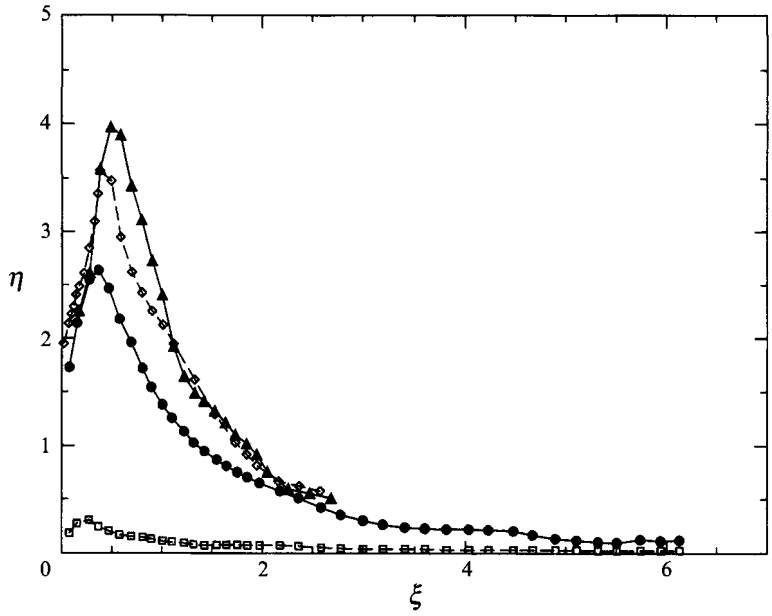

FIGURE 20. Edge-wave amplitudes $\eta = \tilde{\eta}_0/\tilde{\xi}_0(X_T)$ over a beach tilted at angle 0.89° across the channel are compared with those over a plane beach: □, plane beach, 1.2128 s forcing; ●, tilted beach, 1.2128 s forcing; ◇, plane beach, 0.6064 s forcing; ▲, tilted beach, 0.6064 s forcing. Wavemaker stroke $s = 8$ mm.

and 9.54 m in a channel of uniform depth 50 mm. Since the total distance L to the shoreline was approximately 4.69 m it would appear that the seiche was associated with natural periods of oscillation for the tank. These properties suggest that the seiching motion was established as the result of resonant interactions among the various possible modes in the tank. The most likely candidates would appear to be the incident (and or reflected) wave field, the longitudinally radiating field associated with the edge wave and the seiche. However, the appropriate wavenumber and frequency relations for resonance are only very approximately satisfied by this triad. We also considered possible quartets involving transverse waves radiated from the edge-wave field, but these do not fit the resonance criteria at all well.

(Note in review: A referee commented that a seed for the seiche might be supplied in the start-up process of the wavemaker. This is entirely possible as no special precautions were taken with the wavemaker start-up.)

6. Topographical forcing

In addition to the experiment described briefly in § 1 we have made some experiments over a plane beach which had been deliberately tilted across the channel, the angle of tilt being approximately 0.89°, considerably smaller than the 15° slope down the beach. Wave-field measurements were made for wavemaker periods of 0.6064 s and 1.2128 s, the former being a period at which edge waves could readily be generated subharmonically and the latter period corresponds to the natural period of oscillation of the edge wave. The results of such measurements are given in figure 20 where the edge-wave amplitude η is plotted as a function of the scaled offshore distance $\xi = \tilde{\xi}\sigma^2/g \sin\beta$, with σ here taken to be defined by the period 1.2128 s.

For the experiments conducted over the tilted beach at a period of 0.6064 s, measurements of the edge-wave profile were complicated by the fact that the reflected-wave field was skewed to the incident-wave field. The edge-wave field shown in figure 20 was obtained by averaging the transverse-wave amplitudes measured at alternate incident-wave maxima. Notwithstanding this difficulty, the edge wave over the slightly tilted beach had properties similar to those observed over the plane beach, except for the fact that the shorter-period sideband was not observed, and the bandwidth of the marginal stability curve was somewhat reduced, having limits of approximately 0.6014 s and 0.6318 s.

Of greater interest, however, were the wave fields over the beach at an incident-wave period of 1.2128 s. It is seen from the figure that the response forced by the tilted beach was not greatly dissimilar to that observed when the edge waves were generated subharmonically over either the plane or the tilted beach. The synchronously generated waves over the tilted beach were, however, clearly forced by the topographical structure of the beach since, with the standard beach, it is seen from the figure that the edge-wave response was minimal. This experiment must bring into question the interpretation of reported observations that edge waves seen at synchronous forcing periods may have arisen as a consequence of nonlinear wave interactions associated with the longitudinal standing-wave field.

7. Conclusions

The experiments reported herein were carried out to investigate the mechanism by which edge waves may be generated over a plane beach by waves normally incident on the beach from an ocean swell. Because of the large number of modes possible in our simple apparatus, considerable care was needed to delineate carefully the underlying motions whose stability was to be investigated. As indicated in the text, this basic task had several surprises of its own, revealing wave structures we are not able properly to explain at this stage. Nevertheless, a careful mapping of the primary wave field provided a very useful basis for defining an appropriate level of forcing for the subharmonic instability mechanism through which the edge waves were generated. The edge waves thus observed were found to have properties that conformed moderately well with the extant theories, though discrepancies do exist, the reasons for which we do not completely understand at present. One very interesting observation in connection with the generation mechanism was the feature that yet another wave interaction was observed, in which the whole of the tank responded in a seiching mode at certain values of the forcing frequency. The presence of the tank seiche apparently broadened the bandwidth of frequencies over which the instability mechanism was observed in the experiments, making a close comparison with theory difficult to interpret. On the other hand, the initial growth rates of the instability observed experimentally appeared to be significantly larger than was expected theoretically.

It was found in our experiments that edge waves could very easily be generated by the presence of small imperfections at the beach. In one case edge waves were generated quite accidentally by such topographical forcing, and it would therefore appear that, since ocean beaches are never perfectly plane or regular, such a mechanism could be a common source for the generation of edge waves in practical situations.

We are deeply indebted to Dr Janet Becker of the University of California, San Diego, for kindly calculating the theoretical results shown in figures 14 and 16, and for

her helpful comments. The work of W.G.P. was supported in part by the National Science Foundation through award number DMS-9104518 and by a Keck Foundation award.

Appendix. Numerical simulation of the early development of the incident-wave field

Numerical experiments have been made to simulate the measuring procedure used to obtain the data shown in figure 4, which data was measured from wave records of the kind depicted in figure 5. The mathematical model used for these computations is given in (4), with the value of μ chosen to match the decay rate of the steady wave field at a period $T = 0.6064$ s, as shown in figure 6(*a*). The amplitude of the wave field depicted in figure 6(*a*) was found to attenuate at a rate of approximately 0.004 35 per unit depth of water (i.e. at a rate $\zeta^{-1}\,\mathrm{d}\zeta/\mathrm{d}x$, where ζ denotes a wave amplitude, and $x := \tilde{x}/H$ is the distance along the channel). The procedure by which this estimate was made is quite standard, and is described, for example, in Benjamin *et al.* (1987). Such a decay rate is closely matched by the choice $\mu = 0.01$ in (4) and an example of the wave amplitudes at $X = 30.0$, for such a value of μ, is compared in figure 21(*a*) with those found for $\mu = 0$. The numerical experiment from which the results of figure 21(*a*) were obtained simulates the kind of experiment depicted in figure 5, with only the amplitudes of the wave crests being given here.

An interesting feature evident in figure 21(*a*) is that, with no dissipation present, the amplitude of the wave crest settled down only very slowly whereas, with just a small amount of dissipation, the wave amplitude settled to a nearly constant value after only six or seven crests had passed the observation point. This feature was wholly consistent with the experimental observations (cf. figure 5). The input wave amplitude h_0 for these computations corresponded approximately to the amplitude levels associated with the measurements depicted in figure 4(*a*) at a period $T = 0.7400$ s. The influence of different values for the dissipation coefficient μ is also depicted in figure 21(*a*). A value for μ of 0.010 gives approximately the same amount of wave damping as that found in the experiments at the same forcing period T. At larger wave amplitudes similar kinds of results were obtained, as shown in figure 21(*b*) where the magnitudes of the wave crests at $X = 30.0$ are shown for the forcing amplitude $h_0 = 0.06$, which value corresponds to the amplitude levels associated with the experiments of figure 4(*c*) at $T = 0.7400$ s. The wave profile well behind the leading waves at $X = 30.0$, corresponding to the computation shown in figure 22 with $\mu = 0.01$, is given in figure 22. This graph indicates the importance of nonlinear effects on the wave profile at typical amplitudes used in the main experiments. So, for example, we find in this particular case that the wave crest had a magnitude of approximately 0.0567 and the trough of the wave was -0.0462; comparable values for the non-dissipative cases were 0.0651 and -0.0552 respectively. It is interesting that, in the latter case, half the difference between height of the wave crest and the trough was 0.0602, which value coincides very closely with the value of 0.06 used for h_0. This latter property was found to apply very closely in all our numerical experiments, suggesting that the empirical method used to characterize the wave amplitudes (see §3.4) should have given a fairly good representation of the wave fields.

Similar plots of the wave crests at a period $T = 1.2128$ s, near the upper end of the range of measurements for figure 4, are given in figure 23(*a*), and at a period $T = 0.4000$ s, near the lower end of the range, are shown in figure 23(*b*). There is, however, a minor complication associated with the choice of an appropriate value for the

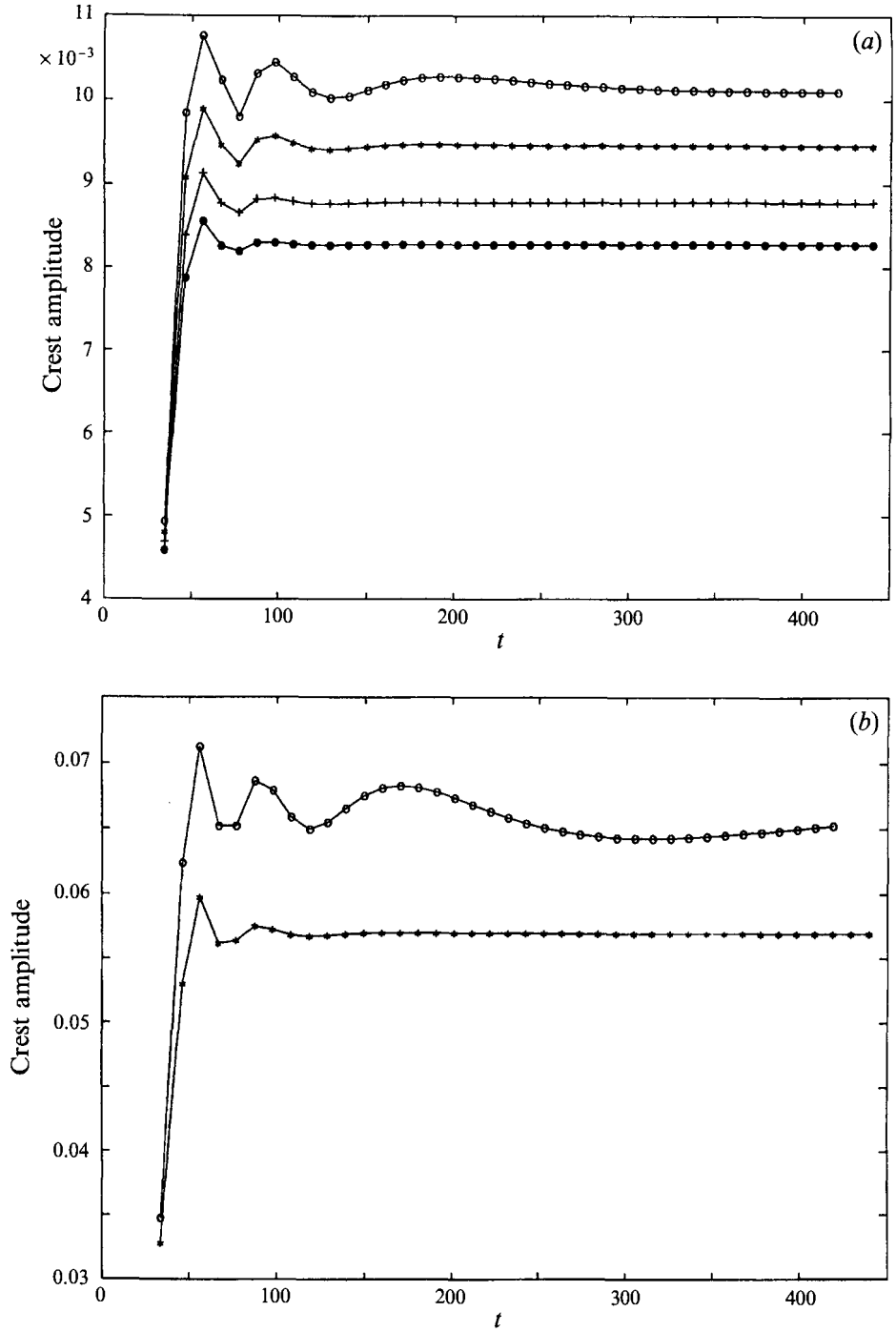

FIGURE 21. The amplitude of the wave crests at $X = 30.0$ for the solution to (4) subject to boundary data $\zeta(0, t) = h_0 \sin \omega t$ with $\omega = 0.6062$ (corresponding to $T = 0.7400$ s). (*a*) $h_0 = 0.01$: ○, $\mu = 0$; *, $\mu = 0.005$; +, $\mu = 0.010$; ●, $\mu = 0.014$. (*b*) $h_0 = 0.06$: ○, $\mu = 0$; *, $\mu = 0.01$.

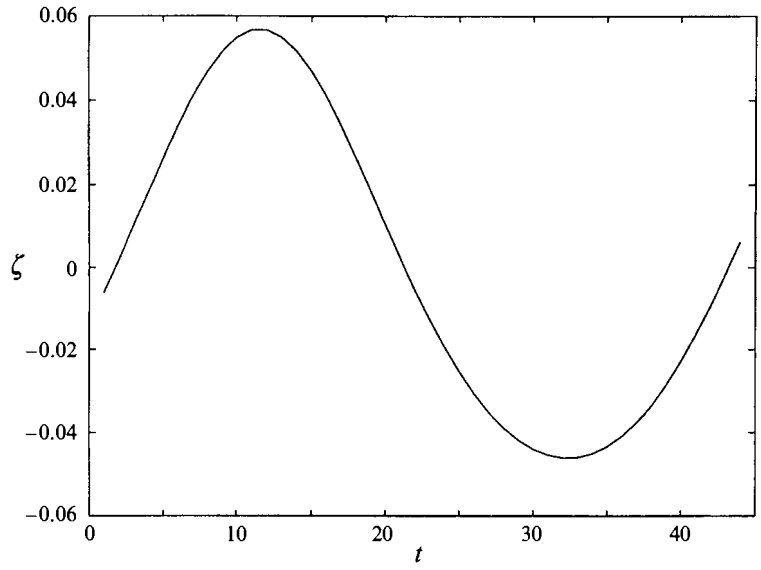

FIGURE 22. The waveform ζ well behind the leading crests (at a time $t_0 \approx 400$) as found at $X = 30.0$ for the solution to (4) subject to boundary data $\zeta(0, t) = h_0 \sin \omega(t + t_0)$, with $h_0 = 0.06$, $\omega = 0.6062$ (corresponding to $T = 0.7400$ s) and $\mu = 0.01$.

dissipative constant μ. The reason is that damping effects arising through dissipation in the boundary layers at the bottom and sidewalls of the channel are proportional to $k^{1/2}$, where k is the wavenumber of the motions. On the other hand, the dissipative operator $\mu\zeta_{xx}$ used in the model equation (4) dampens waves at a rate proportional to k^2. Thus, the constant μ must be adjusted for each wavenumber in order to achieve the amount of damping appropriate to each experiment. In the present computations μ has been scaled by a factor $k^{-3/2}$, using the above-mentioned value $\mu = 0.010$ near the mid-range of the measurements (at $T = 0.7400$ s) on which to base the scaling.

The results shown in figure 23(*a*) for the longer-wavelength motions have similar features to those seen in figure 21(*a*) at $T = 7400$ s, so we have included only the results of the computations corresponding to the largest of the wave amplitudes for figure 4.

For the shorter-wavelength motions (at $T = 0.4000$ s), the computations yielded rather surprising results, as indicated in figure 23(*b*). The non-dissipative model showed considerable variation in the amplitudes of the wave crests at $X = 30.0$, even after 60 or 70 crests had passed the station. It is seen from the figure that the addition of dissipation to the model had the effect of reducing the variation in the amplitude of the wave crests and that, with a value for μ of 0.004, the crests behind the front of the wave train did, indeed, settle down to a nearly uniform level, as was observed in our experiments (see, for example, the waveform shown in figure 5). The value $\mu = 0.004$ should, by virtue of the $k^{-3/2}$-scaling discussed above, correspond approximately to the value appropriate to the experimental conditions at this period. Thus, we see that the wave amplitudes should have been diminished by approximately 50% by the time they reached the observation station at $X = 30.0$. Some caution should, however, be used in making interpretations from these calculations for, at the shorter wavelengths of the experiments, the shallow-water approximation would not have applied very well to the experimental situation. In fact, the ratio of the wavelength to the water depth was only 5 at the period T_1 labelled in figure 4. This feature should have meant there was less dissipation from the boundary layer at the channel bed than would be expected on the

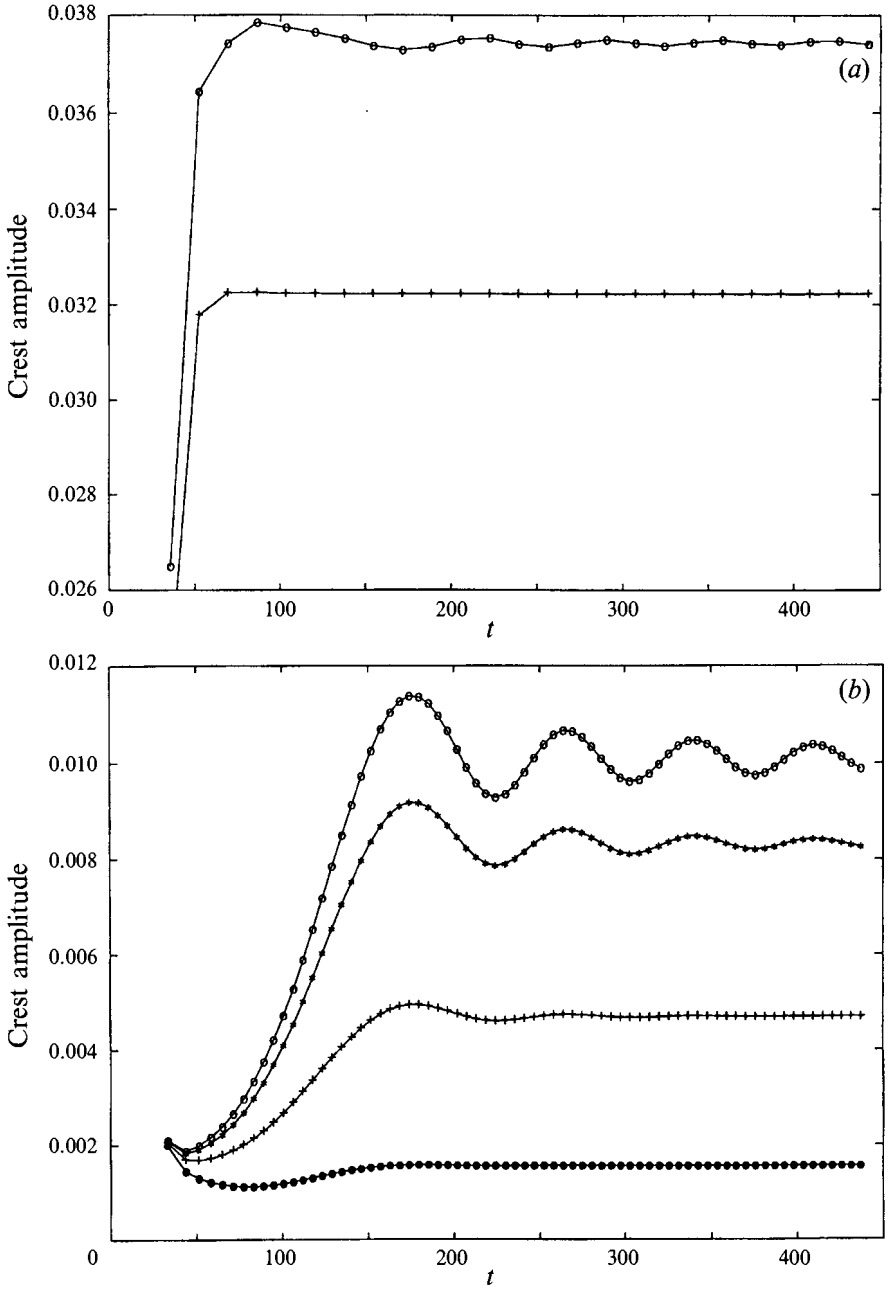

FIGURE 23. The amplitude of the wave crests at $X = 30.0$ for the solution to (4) subject to boundary data $\zeta(0, t) = h_0 \sin \omega t$. (*a*) $h_0 = 0.03$ and $\omega = 0.3699$ (corresponding to $T = 1.2128$ s): ○, $\mu = 0$; +, $\mu = 0.0210$. (*b*) $h_0 = 0.01$ and $\omega = 1.1210$ (corresponding to $T = 0.4000$ s): ○, $\mu = 0$; ∗, $\mu = 0.001$; +, $\mu = 0.004$; ●, $\mu = 0.010$.

basis of a long-wave model (cf. the discussion in §4.1.1); in practice we could also expect somewhat different evolutionary properties for the wave train than that predicted on the basis of the long-wave approximation.

REFERENCES

BENJAMIN, T. B., BOCZAR-KARAKIEWICZ, B. & PRITCHARD, W. G. 1987 Reflection of water waves in a channel with corrugated bed. *J. Fluid Mech.* **185**, 249.

BENJAMIN, T. B., BONA, J. L. & MAHONY, J. J. 1972 Model equations for long waves in nonlinear dispersive systems. *Phil. Trans. R. Soc. Lond.* A **272**, 47.

BIRCHFIELD, G. E. & GALVIN, C. J. JR 1975 Generation of edge waves through nonlinear subharmonic resonance. *Geol. Soc. Am. Mem.* **142**, 15.

BONA, J. L., PRITCHARD, W. G. & SCOTT, L. R. 1981 An evaluation of a model equation for water waves. *Phil. Trans. R. Soc. Lond.* A **302**, 457.

GALVIN, C. J. JR 1965 Resonant edge waves on laboratory beaches. *Eos Trans. Am. Geophys. Union* **436**, 112.

GUZA, R. T. & BOWEN, A. J. 1976 Finite amplitude edge waves. *J. Mar. Res.* **34**, 268.

GUZA, R. T. & DAVIS, R. E. 1974 Excitation of edge waves by waves incident on a beach. *J. Geophys. Res.* **79**, 1285.

GUZA, R. T. & INMAN, D. L. 1975 Edge waves and beach cusps. *J. Geophys. Res.* **80**, 4529.

LIN, N. K. 1988 Excitation of coastal edge waves. *Ocean Phys. Engng* **12**, 65.

MAHONY, J. J. & PRITCHARD, W. G. 1980 Wave reflexion from beaches. *J. Fluid Mech.* **101**, 809.

MATHEW, J. & AKYLAS, T. R. 1990 On the radiation damping of finite-amplitude progressive edge waves. *Proc. R. Soc. Lond.* A **431**, 419.

MILES, J. W. 1990*a* Parametrically excited standing edge waves. *J. Fluid Mech.* **214**, 43.

MILES, J. W. 1990*b* Wave reflection from a gently sloping beach. *J. Fluid Mech.* **214**, 59.

MINZONI, A. A. & WHITHAM, G. B. 1977 On the excitation of edge waves on beaches. *J. Fluid Mech.* **79**, 273.

ROCKLIFF, N. 1978 Finite amplitude effects in free and forced edge waves. *Math. Proc. Camb. Philos. Soc.* **83**, 463.

URSELL, F. 1952 Edge waves on a sloping beach. *Proc. R. Soc. Lond.* A **214**, 79.

URSELL, F., DEAN, R. G. & YU, Y. S. 1960 Forced small-amplitude water waves: a comparison of theory and experiment. *J. Fluid Mech.* **7**, 33.

WEHAUSEN, J. V. & LAITONE, E. V. 1960 Surface waves. In *Handbuch der Physik* (ed. W. Flügge) vol. 9, pp. 446–778. Springer.

YEH, H. H. 1986 Experimental study of standing edge waves. *J. Fluid Mech.* **168**, 291.